Bioorganic Chemistry 166 (2025) 109085

Contents lists available at ScienceDirect

Bioorganic Chemistry

journal homepage: www.elsevier.com/locate/bioorg

New Vanillyl-capped HDAC inhibitors exhibit anti-tumor efficacy in neuroblastoma and glioblastoma cells☆

Ilaria Cursaro [a], Luca Frattaruolo [b], Laura Scalvini [c], Chiara Contri [d], Alessia Bichicchi [e], Nicola Tardiolo [a], Valeria Tudino [a], Sara Rossi [a], Eugenia Nicol Manti [b], Martina Cappello [d], Chiara Papulino [f], Emilia Maellaro [g], Paola Marcolongo [g], Rosaria Benedetti [f,h], Lucia Altucci [f,h,i], Katia Varani [d], Marco Mor [c,j], Maria Frosini [e], Fabrizio Vincenzi [d], Anna Rita Cappello [b], Alessio Lodola [c], Simona Saponara [e], Stefania Butini [a], Gabriele Carullo [a,*], Sandra Gemma [a,*], Giuseppe Campiani [a]

[a] Department of Biotechnology, Chemistry and Pharmacy, University of Siena, Via Aldo Moro 2, 53100 Siena, Italy
[b] Department of Pharmacy, Health and Nutritional Sciences, University of Calabria, Edificio Polifunzionale, 87036 Rende, (CS), Italy
[c] Department of Food and Drug, University of Parma, Parco Area delle Scienze 27/A, Campus Universitario, 43124 Parma, Italy
[d] Department of Translational Medicine, University of Ferrara, Via Luigi Borsari 46, 44121, Ferrara, Italy
[e] Department of Life Sciences, University of Siena, Via Aldo Moro 2, 53100 Siena, Italy
[f] Department of Precision Medicine, University of Campania "Luigi Vanvitelli", Via de Crecchio 7, 80138, Naples, Italy
[g] Department of Molecular and Developmental Medicine, University of Siena, Via Aldo Moro 2, 53100 Siena, Italy
[h] Prof. R. Benedetti, Prof. L. Altucci, Program of Medical Epigenetics, Vanvitelli Hospital, 80138, Naples, Italy
[i] Biogem Institute of Molecular and Genetic Biology, 83031, Ariano Irpino, Italy
[j] Microbiome Research Hub, University of Parma, Parma, Italy

ARTICLE INFO

Keywords:
HDAC inhibitors
neuroblastoma
glioblastoma
apoptosis
cell cycle arrest

ABSTRACT

Histone deacetylases 6 and 8 (HDAC6/8) have emerged as promising therapeutic targets in aggressive neural tumors such as neuroblastoma and glioblastoma. Herein, we report the design, synthesis, and comprehensive biological evaluation of a novel series of hydroxamic acid-based inhibitors (**5a**–**p**), featuring nature-inspired vanillyl CAP groups. Structure–activity relationship (SAR) analysis, supported by molecular docking, elucidated the role of CAP, connecting unit, and linker structure, alongside zinc-binding group orientation, on isoform selectivity and potency. Among the series, compound **5o** emerged as a highly potent and preferential HDAC6 inhibitor (IC_{50} = 4.5 nM). In SH-SY5Y neuroblastoma cells, **5o** induced dose-dependent α-tubulin hyperacetylation, caspase-3/7 activation that indicates apoptosis, a minor autophagy stimulation and showing negligible cytotoxicity in HEK-293 cells. Furthermore, **5o** significantly reduced cell viability in multiple glioblastoma models (U87-MG, T98G, U251-MG), disrupting mitotic progression and promoting G2/M cell cycle arrest, as evidenced by decreased phosphorylation of p-cdc2 (Tyr15). These findings validate the therapeutic relevance of HDAC inhibition in neural tumors and suggest that compound **5o** deserves further investigation as an epigenetic modulator in cancer therapy.

1. Introduction

Histone deacetylases (HDACs) are epigenetic enzymes that control the acetylation status of histones by removing acetyl groups from lysine residues in the *N*-terminal regions of histones. Histone deacetylation strengthens the binding of histones to DNA, leading to a more compact chromatin structure that represses gene transcription, thereby highlighting the role of HDACs as key epigenetic regulators [1]. Mammalian HDACs comprise 18 enzymes grouped into four classes: class I (HDACs 1, 2, 3, and 8), class II, which is subdivided into two groups—class IIa (HDACs 4, 5, 7, and 9) and class IIb (HDACs 6 and 10); class III, or the sirtuin family (SIRT1–SIRT7); and class IV, comprising only HDAC11.

☆ This article is part of a Special issue entitled: 'Targeted cancer therapy' published in Bioorganic Chemistry.

* Corresponding authors.
E-mail addresses: gabriele.carullo@unisi.it (G. Carullo), gemma@unisi.it (S. Gemma).

https://doi.org/10.1016/j.bioorg.2025.109085
Received 30 July 2025; Received in revised form 6 October 2025; Accepted 9 October 2025
Available online 14 October 2025
0045-2068/© 2025 The Author(s). Published by Elsevier Inc. This is an open access article under the CC BY-NC-ND license (http://creativecommons.org/licenses/by-nc-nd/4.0/).

Classes I, II, and IV share the same catalytic zinc ion (Zn^{2+}), which is necessary for the deacetylation reaction, while sirtuins use nicotinamide adenine dinucleotide (NAD^{+}) as a cofactor to exert their catalytic activity [2]. Abnormal HDAC function has been associated with key oncogenic events, with aberrant expression observed in both hematological malignancies [3] and solid tumors [4]. Through the deacetylation of specific proteins, HDACs regulate apoptosis, cell cycle progression, and differentiation [5]. Among HDACs, the class I member HDAC8 is unique, with its gene located on the X chromosome exhibiting both nuclear and cytosolic expression. This distribution enables HDAC8 to deacetylate both histone (e.g., H3) and non-histone proteins, such as structural maintenance of chromosomes 3 (SMC3). Furthermore, the class IIb member HDAC6 is an enzyme predominantly localized in the cytosol, showing preferential deacetylase activity toward non-histone proteins such as α-tubulin and the chaperone HSP90 [6]. Both HDAC6 and HDAC8 are overexpressed in neuroblastoma and glioblastoma, two neurological malignancies that still present unmet therapeutic needs [7,8]. HDAC8 is a prognostic indicator of advanced neuroblastoma, with high metastatic index and poor survival. HDAC6 is upregulated in neuroblastoma metastatic sites and contributes to tumorigenesis by regulating Bax-dependent apoptosis [8]. Moreover, HDAC8 is upregulated in glioblastoma cells, and its downregulation strongly suppresses malignant proliferation by inducing cell cycle arrest and p53-mediated apoptosis [9]. Notably, HDAC6 is deeply involved in glioblastoma, and its aberrant expression facilitates tumor growth [10].

Several HDAC inhibitors (HDACis) have been proposed as tools for the treatment of neurological malignancies [11]. The hydroxamic acid-based HDAC8i PCI-34051 (Fig. 1) promoted apoptosis of neuroblastoma cells, while tubacin, preferentially inhibiting HDAC6, impairs neuroblastoma cells morphology and impeded migration [8].

In glioblastoma, PCI-34051 increases DNA damage and impaired cell cycle progression [12], and tubacin modulates autophagic flux, thereby reducing glioblastoma growth [13]. Although HDAC6is and HDAC8is showed promise in preclinical studies, further research is needed to advance their clinical translation, due to side effects such nausea, vomiting, myelotoxicity, asthenia, cardiac toxicity, anemia and thrombocytopenia [14]. In this context, natural products have emerged as potential HDAC modulators [15,16]. Vanillin and their derivatives were identified as suitable HDAC6is [17], and particularly sinapinic acid (**1**, Fig. 1) displayed in vitro HDAC inhibitory activity comparable to that of valproic acid [18]. Furthermore, synthetic analogues of **1** were described as pan-HDACis, providing critical information for structure-activity relationship (SAR) analyses [19]. Furthermore, other vanillyl- or cinnamyl-based phytochemicals were identified as HDAC8is, like matairesinol (**2**, Fig. 1) and cinnamic acid (**3**, Fig. 1) [20,21]. The development of HDACis based on natural products is a key focus, as reported for belinostat which maintains the cinnamoyl core in its structure [22–25]. In the context of synthetic compounds acting on HDACs, *N*-(4-(hydroxycarbamoyl)phenyl)-*N*-alkylbenzamides, exemplified by MMH409 (**4**, Fig. 1) that is reported as a potent and selective HDAC8i (IC_{50} = 23 nM), are a class of HDACis whose activity can be directed toward HDAC6 and/or HDAC8 by the fine tuning of the size of the alkyl group at the benzamide nitrogen [26]. On the other hand, HDACis selectively targeting HDAC6 and HDAC8 isoforms hold promise for the development of new therapeutics. Recent studies described the development of polypharmacological agents as powerful tools to increase the therapeutic efficacy [27–30]. Specifically, the dual inhibition of HDAC6/HDAC8 may enhance efficacy through synergistic effects [31,32]. Our design strategy leverages the general pharmacophoric structure of HDACis characterized by a zinc binding group (ZBG), and a LINKER portion connecting the ZBG with the surface recognition group, CAP [33,34]. Specifically, the newly developed compounds consist of i) CAP groups derived from different nature-derived scaffolds such as vanilloyl moiety (**5a**–**d**, **5i**–**l**, Fig. 1) or its analogue feruloyl (**5e**–**h**, **5m**–**p**, Fig. 1); ii) a LINKER portion consisting of amide-based moieties (*N*-benzyl or *N*-phenyl), with either the unsubstituted CONH group directing activity against HDAC6, or the CON-*i*Pr moiety guiding the activity toward HDAC8; iii) a ZBG constituted by an hydroxamic acid, in both cases *para*- or *meta*- substituted at the phenyl ring. Specifically, the *p*-substitution proved to be essential for preferential HDAC6 inhibition by leuxinostat (Fig. 1) and its analogues [5]; while, in the case of the dual HDAC6/8 inhibitor BRD73954 (Fig. 1), a phenyl *m*-substituted hydroxamic acid was readily accommodated within the HDAC6 binding groove and was required for HDAC8 inhibition [35].

Thus, we herein describe the development of compounds **5a**–**p** and their ability to inhibit HDAC6 and HDAC8 isoforms. The best performing molecules in terms of preferential HDAC6 or HDAC8 and dual HDAC6/8 activity were further analyzed by assessing their interactions with HDAC1/2/3/5/10/11. Their ability to acetylate histone H3 on lysines 9/14, α-tubulin and SMC3 was also interrogated by western blot. The compounds' anticancer profile was assessed in SH-SY5Y neuroblastoma cells and U87, U251, and T98G glioblastoma cells. Cell cycle analysis, protein expression, Annexin V/propidium iodide assays were performed on **5o** to identify the potential mechanism of cancer cell death. Moreover, a preliminary investigation of the effect of **5o** on autophagy flux in SH-SY5Y cells was performed by determining the LC3II/LC3I ratio and p62 expression.

2. Results and discussion

2.1. Chemistry

Scheme 1 illustrates the synthetic pathway leading to **5a**–**p**. For the preparation of vanilloyl-based derivatives (**5a**–**d**, **5i**–**l**), vanillic acid (**6**) was converted to its corresponding acyl chloride using thionyl chloride and coupled with the appropriate aniline (**17a**,**b**) or benzylamine (**20a**,**b** or **22a**,**b**) under basic conditions to afford amides **7**–**9a**,**b**. These intermediates underwent hydroxylaminolysis by treatment with methanolic hydroxylamine, yielding hydroxamic acids **5a**,**d** and **5k**–**l**. In parallel, *O*-acetylation of **6** furnished carboxylic acid **10**, which followed the same amidation-hydroxylaminolysis reaction sequence to give intermediates **11a**,**b** and, ultimately, **5i**,**j**.

Similarly, for the ferulic-based derivatives (**5e**–**h**, **5m**–**p**), ferulic acid (**12**) was initially *O*-acetylated to yield **13**, which was converted to its corresponding acyl chloride to be reacted with the appropriate aniline (**17a**,**b**) or benzylamine (**20b** or **22a**,**b**) yielding amides **14a**–**c** and **15a**–**d**. Additionally, direct activation of **12** to its acyl chloride, followed by reaction with **20a**, provided **14d**. Intermediates **14a**–**d** and **15a**–**d** were then subjected to hydroxylaminolysis with methanolic hydroxylamine, affording the target compounds **5e**–**h** and **5m**–**p**.

Scheme 2 describes the preparation of key amine and aniline intermediates.

Commercially available 4-aminobenzoic acid (**16a**) and 3-aminobenzoic acid (**16b**) were converted into methyl esters **17a**,**b** through a trimethylsilyl chloride (TMSCl)-assisted esterification reaction in methanol, and later reacted with acetone in a TMSCl/$NaBH_4$-assisted reductive amination reaction to yield the secondary anilines **18a**,**b**. The use of this reductive amination protocol led to improved overall yields. Methyl 4-(aminomethyl)benzoic acid (**19a**) was converted into its corresponding methyl ester **20a** using the same TMSCl-mediated method as described earlier. Meanwhile, 3-cyanobenzoate (**19b**) underwent catalytic hydrogenation in the presence of 12 N HCl to yield the corresponding benzyl amine hydrochloride salt **20b**. Methyl 4-(bromomethyl)benzoate (**21**) and methyl 3-(bromomethyl)benzoate (**21b**) were used in an *N*-isopropylation resulting in the formation of the desired products **22a**,**b** [36]. Compound **4** was prepared as outlined in Scheme 3 [30]. 3,5-Di(trifluoromethyl)benzoic acid (**23**) was activated to the corresponding acyl chloride using oxalyl chloride/DMF and then reacted with **18a** under basic conditions to give **24**. Hydroxylaminolysis of **24**, following general procedure C, furnished compound **4**.

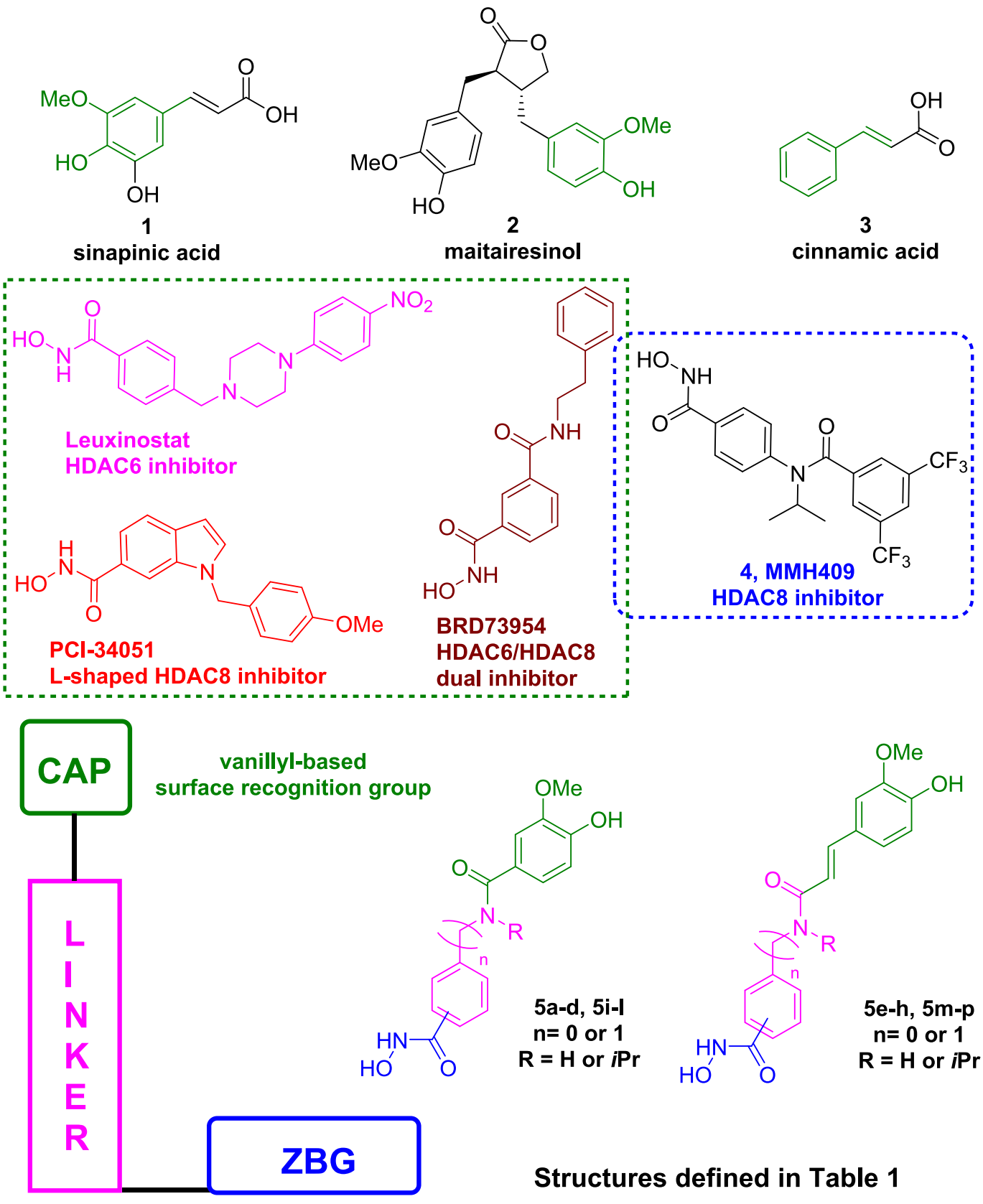

Fig. 1. Structures of reference HDACis and design strategy for the development of new compounds **5a-p**.

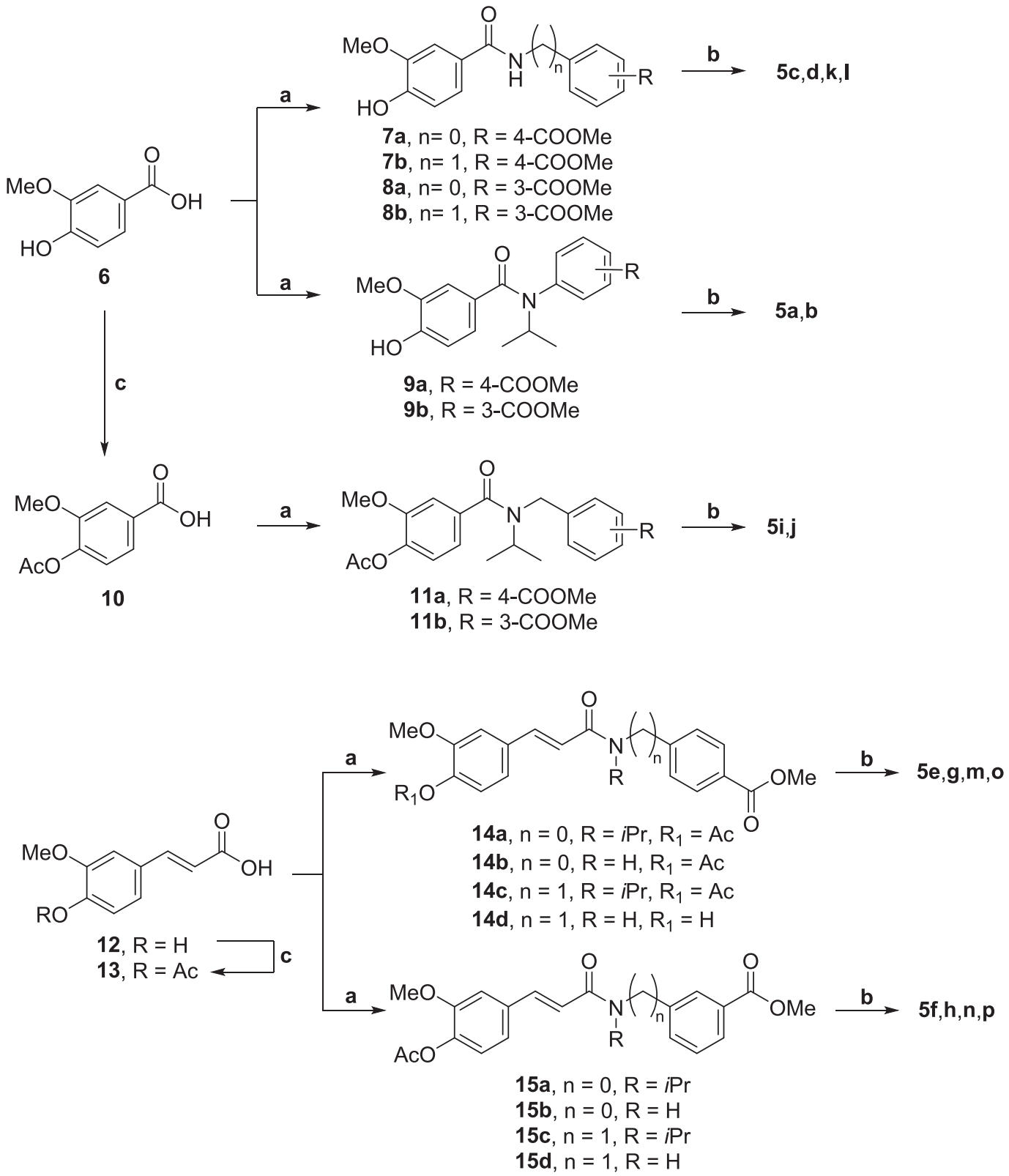

Scheme 1. Reagents and conditions: **a**) step 1. $SOCl_2$, dry DMF, dry DCM, 60 °C, 4 h, 56–99 %, step 2. **suitable aniline or amine**, DIPEA, DCM, 25 °C, 18 h, 24–99 %; **b**) hydroxylamine hydrochloride, KOH, MeOH, 25 °C, 6–18 h, 24–68 %; **c**) Ac_2O, DMAP, Py, 25 °C, 16 h, 99 %.

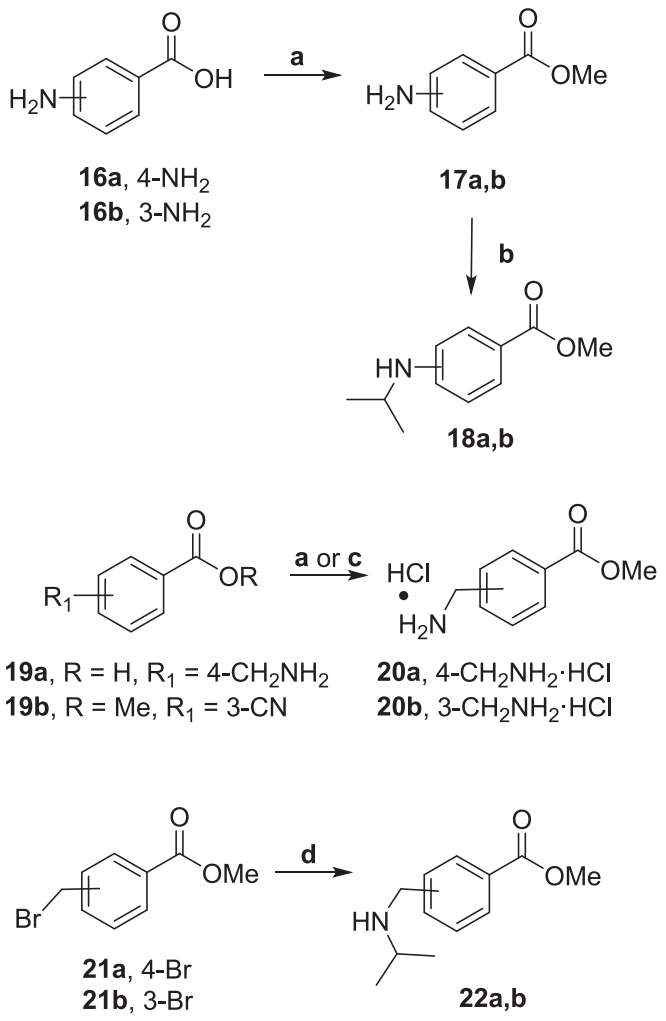

Scheme 2. Reagents and conditions: **a**) TMSCl, MeOH, 25 °C, 18 h, 99 %; **b**) TMSCl, acetone, $NaBH_4$, 0 °C, 20 min, 99 %; **c**) H_2, 12 N HCl, 10 % Pd/C, 25 °C, 3 h, 99 %; **d**) isopropylamine, dry DMF, 25 °C, 16 h, 82–89 %.

2.2. Structure-activity relationship analysis

HDACis usually comprise a ZBG that coordinates the Zn^{2+} at the bottom of the catalytic cavity of the enzyme; a LINKER that occupies the central channel of the enzyme mimicking the acetyllysine substrate; and a CAP group able to explore additional regions of the enzyme near the binding site and often responsible for HDAC subtype selectivity [6]. Our SAR investigation on HDAC6 and HDAC8 inhibition started from *N*-phenylbenzamide **4** (MMH409), recently reported to display high potency and selectivity for HDAC8 (22 nM) [26]. This was selected as a reference compound for our development strategy, and it was resynthesized and tested under the same experimental conditions as for compounds **5**, proving a submicromolar HDAC8 IC_{50} and a limited selectivity over HDAC6, showing a moderate preference (2-fold) for HDAC8 (Table 1). Although experiments were repeated several times, compound **4** (MMH409) never showed the nanomolar potency previously reported elsewhere. On the contrary, PCI-34051 tested in the same experimental conditions, confirmed its nanomolar preferential interaction with HDAC8 ($IC_{50HDAC8} = 10$ nM). The IC_{50} value of 911 nM for **4** in our study is higher than the previously reported value (22 nM). This difference is accounted for by variations in detection technology and assay conditions. In particular, the substantially longer incubation time used in the reference assay [26] (3 h versus 30 min in our protocol) is sufficient to account for this difference in measured potency. To identify new enzyme inhibitors, and taking into account the results obtained with **4**, we initially explored the importance of the CAP group for HDAC6/HDAC8 inhibition by replacing the 3,5-bis(trifluoromethyl) substituents of **4** with 3-methoxy and 4-hydroxy groups, present in the chemical structure of naturally occurring compounds vanillic and ferulic acid. The resulting compound **5a** was inactive on both HDAC isoforms ($IC_{50} > 10$ μM) suggesting that the substitution pattern on the benzamide moiety was critical for the activity. The change in the position of the benzamide fragment with respect to the phenylhydroxamic acid (**5b**) or the removal of the isopropyl group (**5c**) from the benzamide nitrogen did not provide interesting analogues in terms of HDAC8 inhibition but led to an interesting submicromolar activity on HDAC6 (compound **5c**, $IC_{50} = 440$ nM), deserving further attention (vide infra*)*. Inspired by the structures of well-known pan-HDACis panobinostat and belinostat, we expanded our SAR investigation modifying size and shape of the CAP group by preparing vinylogous (*E*)-*N*-phenylcinnamamide derivatives **5e**–**5h**. This exploration led to the identification of two interesting inhibitors with opposite pharmacological profiles. **5e** resulted moderately active on both HDAC6 ($IC_{50} = 5400$ nM) and HDAC8 ($IC_{50} = 1000$ nM), whereas **5f** showed increased potency in blocking HDAC6 ($IC_{50} = 54$ nM) and, to a lesser extent, HDAC8 ($IC_{50} = 820$ nM). The experience gained in the design and synthesis of HDAC6 inhibitors [37] prompted us to *i)* increase molecular flexibility by passing from rigid (*E*)-*N*-phenylcinnamamide derivatives to (*E*)-*N*-benzylcinnamamides and *ii)* replace the bulky isopropyl group with a simple hydrogen atom. Both strategies contributed to the improvement of the inhibitory potency on HDAC6 with **5m** displaying an $IC_{50} = 29$ nM and **5o** emerging as single digit nanomolar inhibitor of HDAC6 ($IC_{50} = 4.5$ nM) with a nearly 1000-fold HDAC6/HDAC8 selectivity. Considering the remarkable inhibitory activity displayed by the (*E*)-*N*-benzylcinnamamide **5o** on HDAC6, we set to rationalized SAR data on this isoform by means of computational analysis exploiting the X-ray structure of the catalytic domain of *h*HDAC6 in complex with trichostatin A (PDB id: 5EDU) [38]. Docking simulations showed that **5o** perfectly fits within the catalytic site of *h*HDAC6 (Fig. 2A) with the hydroxamic acid group, modelled in neutral form, able to chelate the zinc atom, and its polar benzamide hydrogen forming a hydrogen bond with Ser568. The targeting of this residue,

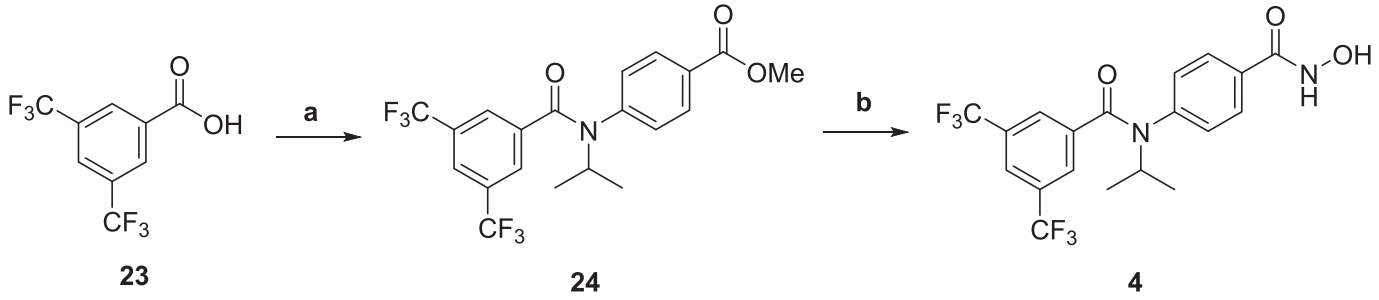

Scheme 3. Reagents and conditions: **a**) step 1. $(COCl)_2$, DMF, dry DCM, rt., 2 h, step 2. **18a**, DIPEA, DCM, 16 h, rt., 56 %; **b**) hydroxylamine hydrochloride, KOH, MeOH, rt., 12 h, 55 %.

Table 1
Inhibitory Activity of compounds **5a**–**p** toward *h*HDAC6 and *h*HDAC8 (as IC_{50}, nM)[a].

Cpd	Structure	*h*HDAC6	*h*HDAC8	Cpd	Structure	*h*HDAC6	*h*HDAC8
5a	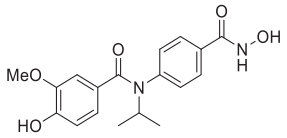	>10,000 (25 %)	>10,000 (15 %)	**5i**	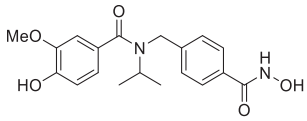	839 ± 55	>10,000 (11 %)
5b	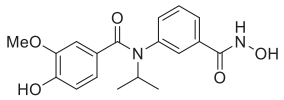	>10,000 (20 %)	>10,000 (9 %)	**5j**	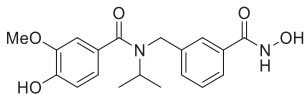	3115 ± 241	>10,000 (8 %)
5c	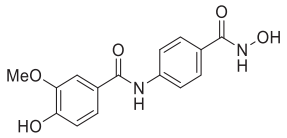	442 ± 32	3155 ± 211	**5k**	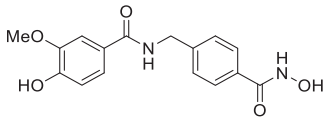	32 ± 2	5852 ± 328
5d	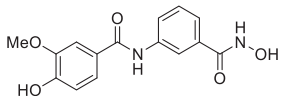	>10,000 (1 %)	>10,000 (5 %)	**5l**	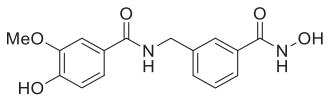	2440 ± 157	>10,000 (39 %)
5e	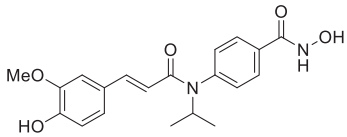	5430 ± 329	989 ± 67	**5m**	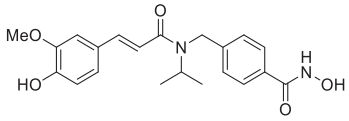	29 ± 2	831 ± 57
5f	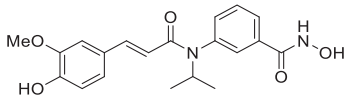	54 ± 4	820 ± 61	**5n**	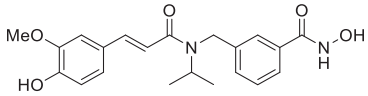	7560 ± 458	>10,000 (34 %)
5g	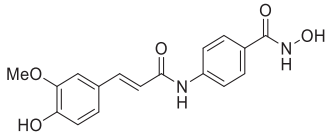	453 ± 32	2354 ± 168	**5o**	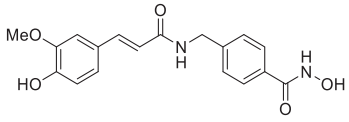	4.5 ± 0.32	3273 ± 244
5h	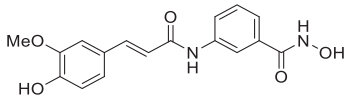	573 ± 41	2818 ± 139	**5p**	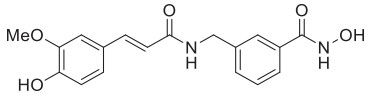	706 ± 48	1562 ± 108
4 (MMH409)[b]		1863 ± 121	911 ± 7	**Panobinostat**[c]		9.55 ± 0.67	423 ± 31
SAHA[c]		33 ± 2	854 ± 63				

[a] Each value is the mean of at least three determinations; results are expressed as mean ± standard error of the mean (SEM).
[b] MMH409 (**4**) was resynthesized and tested under the same experimental conditions as for compounds **5a**–**p**.
[c] SAHA and Panobinostat were tested under the same experimental conditions as for compounds **5a**–**p.**

located at the rim of the catalytic pocket of the HDAC active site, has been reported as a general strategy to obtain potent and selective HDAC6is [39,40]. What is more, the 3-methoxy-4-hydroxyl-cinnamoyl moiety of **5o** undertakes both π-π and polar interactions with aromatic and polar residues, respectively, located at HDAC6 active site entrance. The reported binding mode qualitatively accounts for the moderate loss in HDAC6 activity displayed by the corresponding *N*-isopropyl derivative **5m** (Fig. 2B), and for the most significant one displayed by the (*E*)-*N*-benzylcinnamamide positional isomer **5p** (Fig. 2C). In these cases, the title compounds are unable to form a H-bond with Ser568, although alternative polar contacts (i.e. involving Asp497) may somehow compensate for the absence of this important interaction. Finally, the docking pose of **5o** also accounts for the reduced activity displayed by the *N*-benzamide **5 k** analogue (not shown here), which fails to occupy all the available space of the HDAC6 binding pocket. Analogues **5e,f,k, m,o**, emerged as the best HDAC6 or HDAC8 inhibitors, were further investigated for selectivity against other members of class I enzymes and HDAC10 isoform. The HDAC6is **5f-5o**, displayed some activity also on other HDAC isoforms but with inhibitory potency approaching (**5o**) or overcoming (**5f-5 m**) the micromolar range. Conversely, the HDAC8i **5e** resulted more potent at inhibiting HDAC1 than HDAC8 or the other considered HDAC isoforms. Considering HDAC1, **5e** demonstrated a preferential binding against HDAC1 isoform if compared with potency against HDAC6/8 and **5f**, a dual HDAC6/8 inhibitor, showed against HDAC1 with a IC_{50} much lower than that for HDAC6. **5k** and **5m** confirmed their preferential inhibitory activity against HDAC6. When tested against HDAC2 and HDAC3, **5e** demonstrated a noteworthy selectivity against HDAC1 within the class I isoforms, while **5m** showed micromolar IC_{50}s against HDAC1–3, confirming its preferential binding to HDAC6. Moreover, **5e,f** did not show appreciable binding properties against HDAC10 isoform, while **5k** and **5m** showed a potency in the micromolar range, similar to that against class I enzymes. Furthermore, **5m**, **5o** and reference compound **4** were tested against HDAC5 (class IIa member) and HDAC11 (class IV). They showed a high micromolar

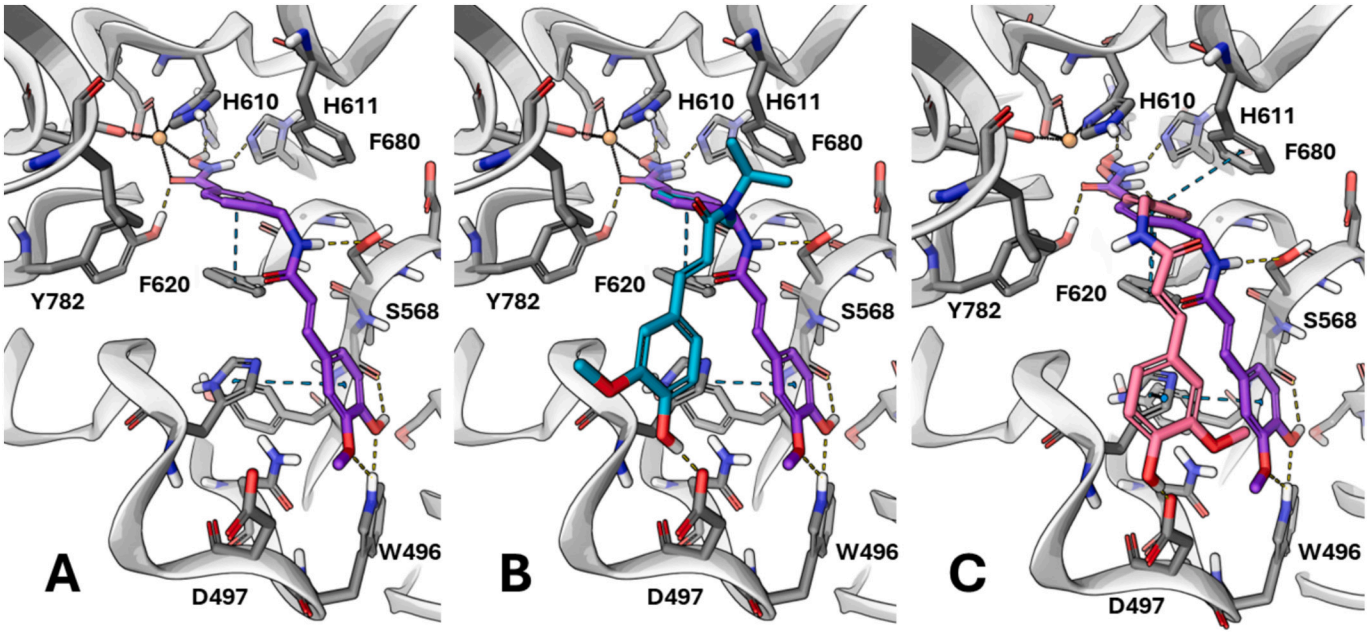

Fig. 2. Docking poses of selected N-benzylcinnamamide derivatives 5 m, 5o, and 5p within HDAC6 (white cartoon and gray carbon atoms, with Zn atom shown as an orange sphere). Panel A reports the top-ranked pose for compound **5o** (violet caron atoms), while panel B and C reported the top-ranked poses for **5 m** (cyan carbon atoms) and **5p** (pink carbon atoms), respectively. Coordination-bonds are displayed as tiny black points, H-bonds are represented as yellow dotted lines while π-π interactions as blue dotted lines. (For interpretation of the references to colour in this figure legend, the reader is referred to the web version of this article.)

potency of inhibition against HDAC5 (**5m** IC_{50} = 2633 nM and **5o** IC_{50} = 4455 nM) while they did not display appreciable inhibition for HDAC11. Interestingly, **4** showed a micromolar potency against HDAC11 with an IC_{50} value of 8228 nM. In general **5o**, tested against the whole panel of enzymes, showed a submicromolar potency against isoforms HDAC1–3,10, confirming its preferential binding to HDAC6.

2.3. Target engagement in cells: acetylation profile of target proteins α-tubulin, SMC3, histone H3 Lys9/14

The best performing compounds in terms of HDAC inhibition profile were **5e** (preferential HDAC1/8 inhibitor), **5f** (HDAC1/6/8i), **5k** (preferential HDAC6i), **5m** (HDAC6/8i) and **5o** (preferential HDAC6i). To assess the HDAC modulation of these compounds, we performed Western blot experiments in living cells. The cell-based assays were conducted on human SH-SY5Y neuroblastoma cells, a cell line stably expressing class I (i.e., HDAC1 and HDAC8) and class II (i.e., HDAC6) enzymes [41]. We evaluated the levels of α-tubulin acetylation (the client protein of HDAC6), acetylation of histone H3 (the primary substrate of HDAC1–3) and levels of acetylated SMC3 (non-histone substrate of HDAC8) after incubation of compounds **5e**, **5f**, **5k**, **5m** and **5o** at two different concentrations, 1 and 10 μM for 24 h, in comparison

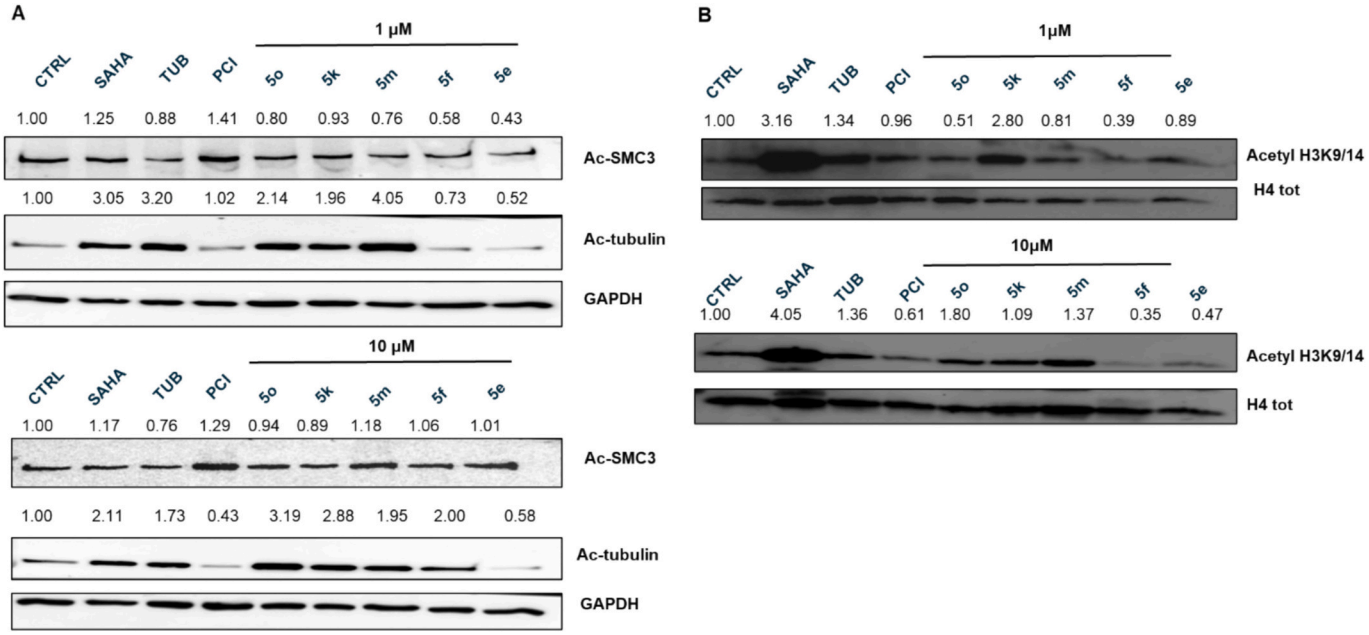

Fig. 3. Western blot analysis of acetylated α-tubulin expression on the total protein extract and evaluation of H3 total acetylated expression on the histone extract. Densitometric analysis was assessed throughout ImageJ software (version 1.44).

with vorinostat or SAHA, used as pan-HDACi, tubastatin A (TUB), generally used as HDAC6i, and PCI34051(PCI), recognized HDAC8i. Compound **5e** was not able to modify the acetylation levels of α-tubulin and SMC3 at both tested concentrations indicating that this N-isopropyl benzanilide derivative failed to engage both HDAC6 and HDAC8 in intact cells(Fig. 3A).

The analogue **5f** induced an appreciable acetylation of α-tubulin at 10 μM, but not of SMC3, thus indicating its ability to interact with HDAC6 but not with HDAC8 in SH-SY5Y cells (Fig. 3A). Compound **5k** induced a dose-dependent acetylation of α-tubulin, thus confirming HDAC6 interaction, with no effect on SMC3 (Fig. 3A). **5m** was able to induce strong acetylation of α-tubulin and of SMC3 (although at a marginal extent), emerging as the only compound of the series able to pharmacologically interact with HDAC6 and HDAC8 in cells (Fig. 3A). Finally, the potent HDAC6i **5o**, was able to promote acetylation of α-tubulin in a dose-dependent manner, thus confirming its ability to specifically engage HDAC6 also in SH-SY5Y cells (Fig. 3A-B). To further analyze the cellular engagement of class I HDACs, we measured the acetylation levels of histone H3 Lys 9/14, marker of specific class I HDAC inhibition. As reported in Fig. 3B, none of the newly synthetized compounds reached the level of histone H3 acetylation observed with SAHA. Only compound **5k** was able to promote a slight increase of H3K9/14 acetylation. Overall, **5o** emerged as a functionally selective HDAC6i and **5m** as a dual HDAC6/HDAC8i, with limited effects on histone targets in cells. The compounds selected for biological evaluation were also tested for their cytotoxicity in HEK-293 cells (**Fig. S1**). Compounds **5e**, **5f**, **5k**, and **5m** did not show significant cytotoxicity at any of the tested concentrations (10 nM – 30 μM), after 24 h of exposure. Similarly, compound **5o** did not induce any appreciable reduction in cell viability even after 72 h of treatment. In contrast, the known HDACi SAHA exhibited a significant cytotoxic effect at 10 and 30 μM after 72 h (**Fig. S1**).

2.4. Therapeutic potential of newly developed HDACis

Based on both IC_{50} data reported in Tables 1,2 and target engagement experiments shown in Fig. 3, we selected **5e** (inhibitor of HDAC1/8), **5m** (inhibitor of HDAC6/8) and **5o** (inhibitor of HDAC6) for further analysis as potential antitumor tools in neuroblastoma and glioblastoma cells. In particular, the SH-SY5Y neuroblastoma cells were included in the investigation because they stably express HDAC enzymes and are reported in literature for their prevalent role as cellular models to study the effects of new drugs in neuroblastoma, including HDACis, as outlined for SAHA and different hydroxamic acids [8].On the other hand, for studying the effects of new compounds on glioblastoma, we selected three different cell lines named U87-MG, T98G and U251-MG, which represent gold standard cells used to test the effects of new compounds on glioblastoma growth and express both class I and class II HDACs. Of note, several pan-HDACis were tested in these cell lines showing to promote cancer cell death modulating different epigenetic and non-epigenetic pathways [42,43].

2.5. Efficacy of newly developed HDACis in neuroblastoma SH-SY5Y cells

The selected HDACis were tested in SH-SY5Y cells in MTT assay to assess the reduction of cell viability. **5m**, **5o**, and SAHA (reference compound) caused a concentration-dependent reduction in SH-SY5Y cell viability (Fig. 4), whereas **5e** was ineffective up to 100 μM concentration thus confirming its role as a negative control because it was not able to modulate the acetylation of both histone and non-histone markers. **5o** showed the best performing profile in SH-SY5Y cells with a IC_{50} value of ~ 3 μM. To determine whether cell death is associated to apoptotic mechanisms, including DNA fragmentation, subsequent DNA loss, and alterations in cell cycle progression, flow cytometry analysis was conducted on **5m** and **5o**. SH-SY5Y cells treated with both compounds at concentrations close to their IC_{50} values and compared to the effects of SAHA. As illustrated in Fig. 5, all tested compounds led to an accumulation of hypodiploid SH-SY5Y cells in the subG0/G1 phase (~ +10 %), accompanied by a decrease in the G0/G1 population and a slight increase in cells within the S-phase (**5o**) or G2/M-phase (**5m**), suggesting that, under these conditions, these compounds trigger programmed cell death in SH-SY5Y cells.

2.6. Evaluation of apoptosis in SH-SY5Y cells

To confirm the induction of apoptosis and to discriminate between early and late apoptotic events, we used the Annexin V/Sytox staining followed by flow cytometry analysis, performing the experiments on SH-SY5Y cells treated with compound **5o** or SAHA at 3, 10 and 30 μM (Fig. 6).

Different time points and concentrations were employed to optimize treatment conditions and ensure reliable detection of apoptosis by Annexin V/Sytox assay, as apoptotic responses can vary depending on the intensity and duration of the cytotoxic stimulus. At 24 h, **5o** induced a concentration-dependent increase in early apoptosis, reaching statistical significance at concentrations of 10 μM and 30 μM. SAHA showed a more potent effect, significantly increasing early apoptotic cells even at 3 μM. A similar trend was observed for late apoptosis, with significant increases starting at 10 μM for **5o** and at all tested concentrations for SAHA (Fig. 6). We further analyzed the apoptotic profile after 48 h and 72 h of treatment; at 48 h of treatment, both early and late apoptosis levels further increased, with **5o** showing significant effects at 10 μM and a pronounced apoptotic response at 30 μM (46 % for early and 27 % for late apoptosis), similar, though slightly lower, to those observed with SAHA. At 72 h, the pro-apoptotic effect of **5o** became even more pronounced: early and late apoptosis significantly increased at all concentrations, reaching levels comparable to those induced by SAHA (Fig. 6). Based on these findings, compound **5o** demonstrates a clear time- and concentration-dependent pro-apoptotic activity in SH-SY5Y neuroblastoma cells that closely parallels that of SAHA. To confirm the activation of the apoptotic cascade, we next measured caspase-3/7 activity in SH-SY5Y cells treated with **5o** or SAHA under the same experimental

Table 2
Inhibitory Activity of compounds **5e,f,k,m,o** toward a panel of HDAC enzymes (as IC_{50}, nM)[a].

Cpd	*h*HDAC1	*h*HDAC10	*h*HDAC2	*h*HDAC3	*h*HDAC5	*h*HDAC11
5e	312 ± 22	>10,000 (33 %)	>10,000 (29 %)	>10,000 (32 %)	NT[b]	NT[b]
5f	825 ± 66	>10,000 (29 %)	NT[b]	NT[b]	NT[b]	NT[b]
5k	1282 ± 93	1185 ± 84	NT[b]	NT[b]	NT[b]	NT[b]
5m	1488 ± 117	1136 ± 82	3236 ± 224	1840 ± 124	2633 ± 153	>10,000 (46 %)
5o	403 ± 31	202 ± 14	537 ± 38	127 8	4455 ± 257	> 10,000 (42 %)
4[b]	NT[b]	NT[b]	>10,000 (41 %)	>10,000 (45 %)	>10,000 (4 %)	8228 ± 543
Panobinostat[c]	63 ± 4	6.38 ± 0.47	36 ± 3	3.95 ± 0.22	NT[b]	NT[b]
SAHA[c]	284 ± 21	139 ± 8	123 ± 7	12.6 ± 0.9	NT[b]	NT[b]

[a] Each value is the mean of at least three determinations; results are expressed as mean ± standard error of the mean (SEM).
[b] NT: not tested.
[c] SAHA and Panobinostat were tested under the same experimental conditions as for compounds **5e,f,k,m,o** and **4.**

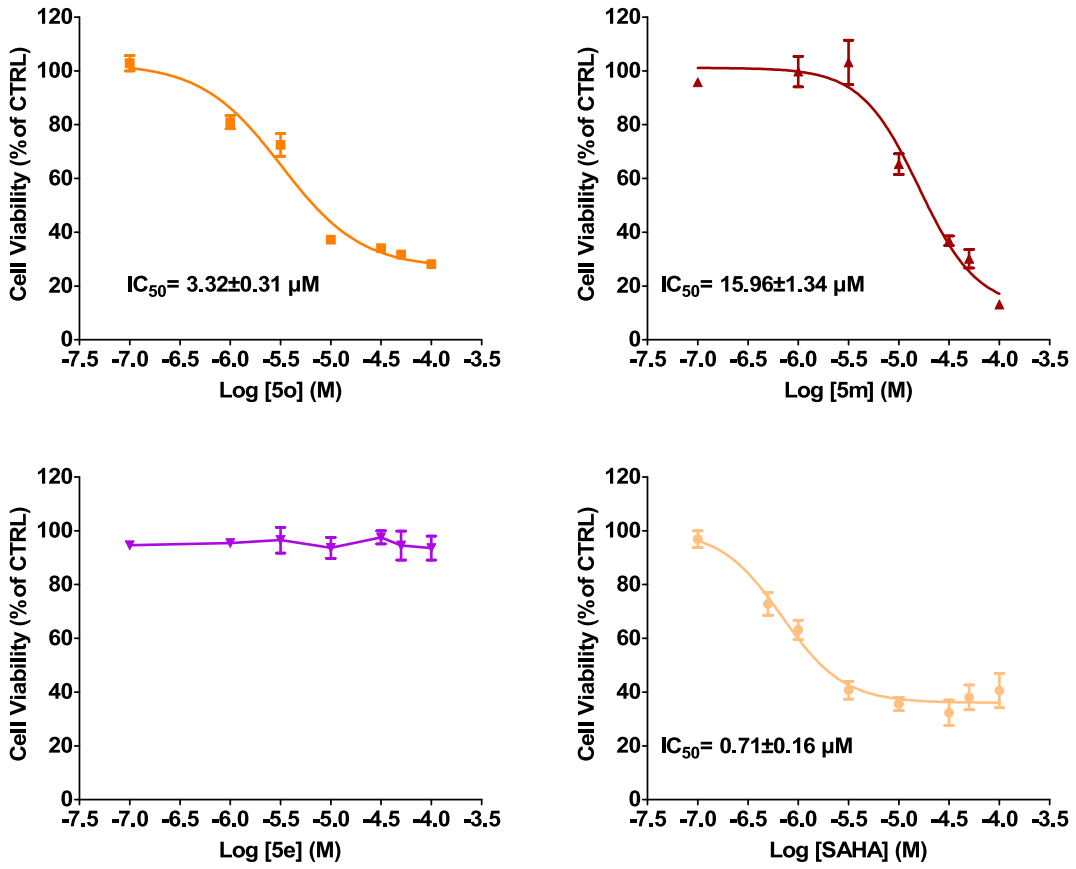

Fig. 4. Effects of **5o**, **5 m**, **5e**, and SAHA on SH-SY5Y cell viability. Cells were incubated with increasing concentrations of the compounds and MTT test was performed at 24 h. Data are reported as mean ± SEM of at least three independent experiments.

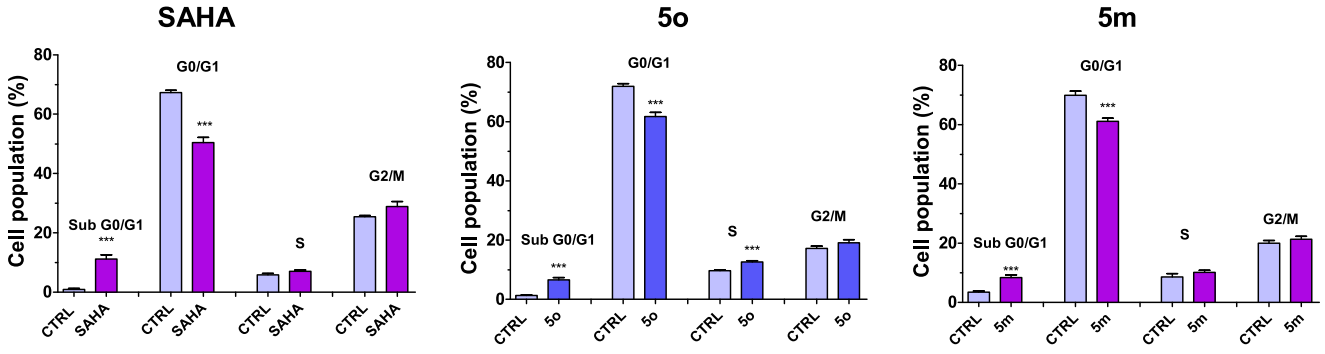

Fig. 5. Effects of SAHA, **5o** and **5 m** on the human SH-SY5Y neuroblastoma cells cycle distribution. Cells were treated for 24 h at concentration close to their IC_{50} extrapolated by MTT assay (for SAHA and **5o**, 3 μM; **5 m**, 15 μM). Percentages of cells in subG0/G1, G0/G1, S, and G2/M phases are reported as means ± SEM of at least three independent experiments run in triplicates. *** $p < 0.001$ vs. CTRL, same cell cycle phase (unpaired Student *t*-test).

conditions. At 24 h, both **5o** and SAHA induced a concentration-dependent increase in caspase-3/7 activation, with significant effects observed starting from 10 μM. At the highest concentration tested (30 μM), **5o** and SAHA elicited similar levels of caspase-positive cells (24 % and 26 %, respectively), indicating a similar ability to engage the apoptotic cascade at this early stage (Fig. 7). At 48 h, caspase activation became more prominent, with **5o** showing a significant increase in caspase activation at 10 μM and 30 μM, while SAHA showed this profile at all the tested concentrations. After 72 h, **5o** continued to activate caspase-3/7 in a concentration-dependent manner, with 43 % positivity at 30 μM, closing approaching the effect of SAHA (51 %) at the same concentration (Fig. 7). The observed increase in caspase-3/7 activity further supports the conclusion that **5o** activates the intrinsic apoptotic cascade, confirming that the observed cell death is apoptotic in nature rather than necrotic or non-specific. Notably, at 30 μM and 72 h, **5o** approaches the pro-apoptotic efficacy of SAHA, suggesting that it may represent a promising candidate for further investigation as a potential anticancer agent targeting neuroblastoma cells. Since **5o** showed a strong reduction in cell viability at 24 h of incubation as indicated by MTT assay (Fig. 4), with a limited induction of apoptosis, we investigated the effect of **5o** on autophagy [44].

Pan-HDACi SAHA has been proven to induce autophagy [45], thus we tested the effect of 3 μM **5o** in comparison with 3 μM SAHA (positive control). After 24 h of treatment with or without chloroquine (CQ, a known autophagy modulator), we measured LC3-II/LC3-I ratio and p62/SQSTM1 levels (**Fig. S2**), as two of the most important autophagy

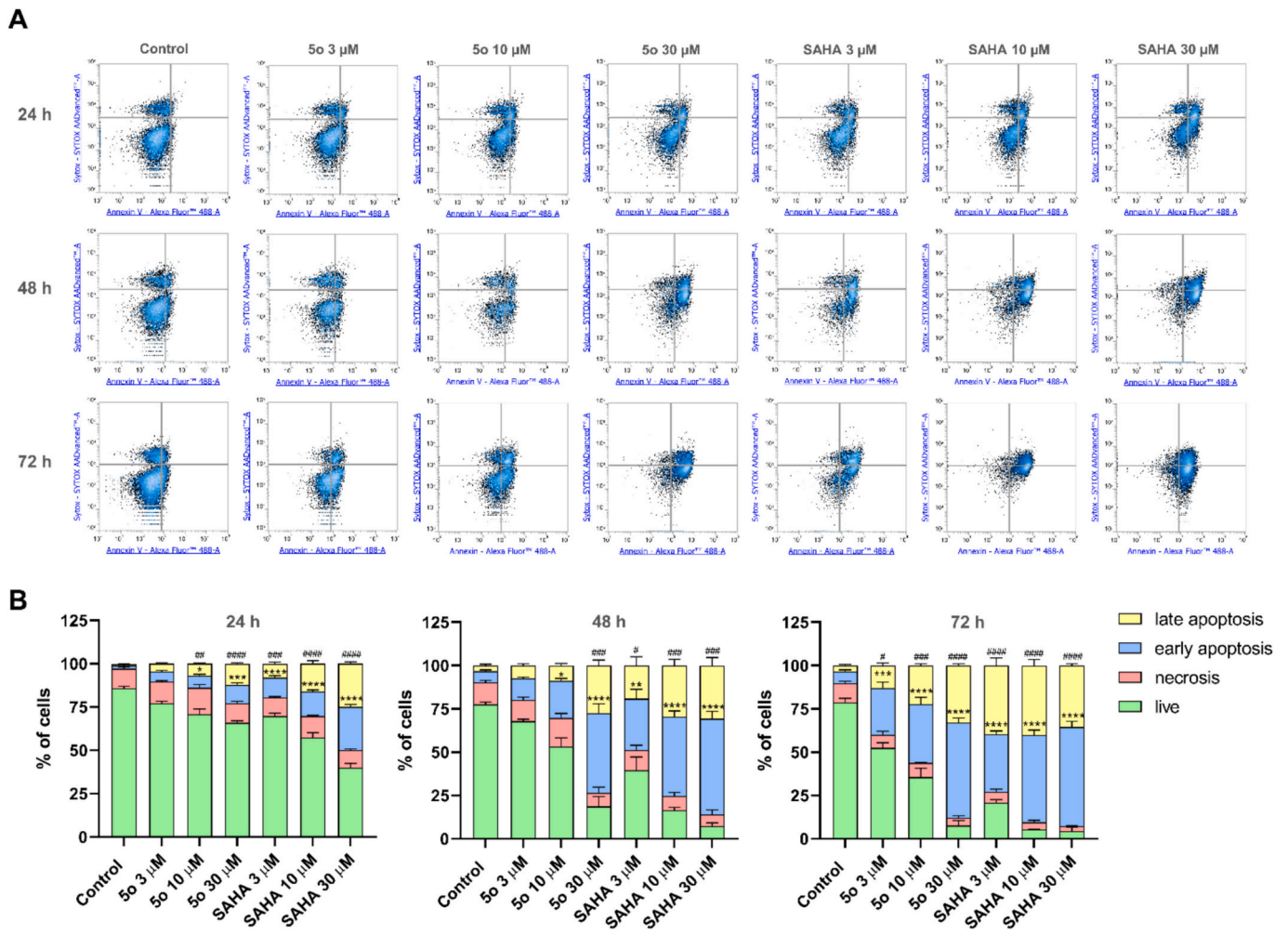

Fig. 6. Effects of **5o** and SAHA on SH-SY5Y cell apoptosis. (A) Representative flow cytometry dot plots showing Annexin V and Sytox staining after 24, 48 and 72 h of treatments with the indicated concentrations of compounds. Early apoptotic cells (Annexin V^+/$Sytox^-$) and late apoptotic cells (Annexin V^+/$Sytox^+$) were identified based on their localization in the lower right and upper right quadrants of the dot plots, respectively. (B) Quantification of cell populations shown as stacked bar graphs, representing the percentage of live, necrotic, early apoptotic, and late apoptotic cells at 24, 48 and 72 h under the indicated conditions. Data are presented as mean ± SEM from $n = 3$ independent experiments. Statistical significance was assessed by one-way ANOVA followed by Dunnett's multiple comparisons test. Asterisks (*) indicate statistical significance for early apoptosis (*, $p < 0.05$, **, $p < 0.01$, ***, $p < 0.001$ and ****, $p < 0.0001$ vs control); hash symbols (#) indicate significance for late apoptosis ($^{\#}$, $p < 0.05$, $^{\#\#}$, $p < 0.01$, $^{\#\#\#}$, $p < 0.001$ and $^{\#\#\#\#}$, $p < 0.0001$ vs control).

markers. Increased levels of LC3-II and LC3-II/LC3-I *ratio* indicate autophagy stimulation, especially if such increase is confirmed and amplified by CQ co-treatment, which blocks the final degradation phase. As regards p62/SQSTM1, this protein acts as a cargo receptor for autophagic degradation of polyubiquitinated target molecules, and in doing so it is itself degraded in autophagolysosomes. Thus, increased levels of p62 in cells co-treated with CQ confirm the occurrence of an actual autophagic flux. As shown in **Fig. S2**, in CQ co-treated cells SAHA induced an increase of LC3-II/LC3-I ratio and a significant increase of p62 levels compared to untreated cells, while these changes were smaller and not statistically significant in cells treated with **5o**. Based on these findings, in SH-SY5Y cells under the tested conditions, the reference compound SAHA proved to be a moderate autophagy inducer; on the contrary, **5o** induces a minor autophagy stimulation**,** despite its marked antitumor activity observed at 24 h in the MTT assay.

2.7. Efficacy of newly developed HDACis in U87-MG, T98G and U251-MG glioblastoma cells

The newly synthesized HDACis **5e**, **5m** and **5o**, as well as SAHA, were tested on three different glioblastoma cell lines in order to assess their ability to affect the proliferation of this malignancy (Table 3 and Fig. 8), which is the most common brain cancer in adults [46]. Firstly, the activity of the different molecules in inhibiting cell proliferation was evaluated. For this purpose, three different cell lines, namely U87-MG, T98G and U251-MG, were exposed at increasing concentrations of the different compounds for either 24 or 72 h.

Although no inhibitory effects on cell viability/proliferation were detected after 24 h of treatment, after 72 h a clear dose-dependent effect of the compounds **SAHA**, **5o** and **5m** was observed, while **5e** proved to be ineffective. **Table 4** (which report the IC_{50} values) and Fig. 8A, highlighted slight differences in the activity of the different compounds. Moreover, the results demonstrated a remarkable difference in the sensitivity of different glioblastoma cell lines to HDACis, with the U251-MG cell line being the most responsive to both SAHA and the newly synthesized compounds. This finding is consistent with the literature which shows the variable expression of HDAC isoforms among different gliobastoma cell lines, and in particular the higher activity of newly synthesized compounds in U251-MG cells is in line with the higher expression levels of the HDAC6 isoform reported for this cell line [47].

The study was further extended by monitoring the effects of the synthesized compounds on the cell cycle of glioblastoma lines, and the

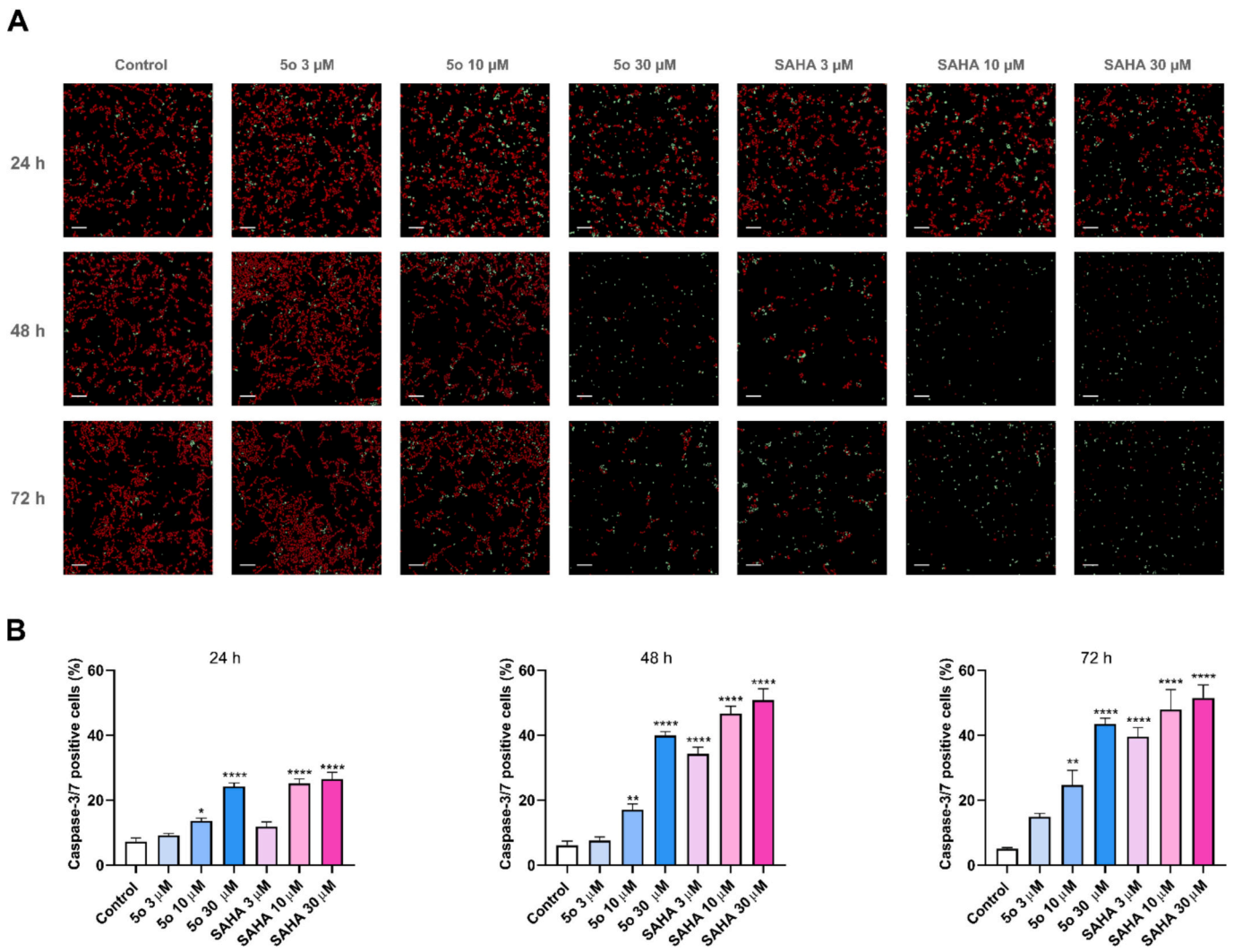

Fig. 7. Effects of **5o** and SAHA on caspase-3/7 activation in SH-SY5Y cells. (A) Representative fluorescence images (10× magnification) showing SH-SY5Y cells stained for caspase-3/7 activity after 24, 48 h and 72 h of treatment with the indicated concentration of compound **5o** and SAHA. Caspase-3/7–positive cells appear in green while caspase-3/7–negative cells are shown in red. Scale bar = 150 μm. (B) Quantification of caspase-3/7–positive cells after 24, 48 and 72 h of incubation with compound **5o** or SAHA. Data are presented as mean ± SEM from $n = 3$ independent experiments. Statistical significance was assessed by one-way ANOVA followed by Dunnett's multiple comparisons test. *, $p < 0.05$ **, $p < 0.01$ and ****, $p < 0.0001$ vs control. (For interpretation of the references to colour in this figure legend, the reader is referred to the web version of this article.)

Table 3
Antiproliferative activity of tested compounds.

Cell lines	SAHA	5o	5 m	5e
U87-MG	12.56 ± 2.51	51.31 ± 5.8	18.68 ± 3.52	>100
T98G	3.64 ± 0.85	42.60 ± 4.83	25.03 ± 6.75	>100
U251-MG	1.76 ± 0.37	2.37 ± 0.65	2.3 ± 0.75	>100

Data are presented as IC_{50} values (μM) ± SEM from $n = 3$ independent experiments.

results obtained were compared to those induced by the well-known HDACi SAHA. The results obtained, shown in Fig. 8B, revealed the ability of the compounds to affect cell cycle progression, causing a reduction of G0/G1 cell population and an increase of the G2/M population. This result aligns with previously published results that report similar behavior for other HDACis [48,49]. Cell cycle arrest mediated by the different inhibitors was further corroborated by assessing the phosphorylation levels of cyclin-dependent kinase 1 (p-cdc2), which plays a key role in cell cycle progression. As shown in Fig. 8C, treatment with the compounds resulted in decreased phosphorylation of cdc2 at tyrosine 15 (p-cdc2 Tyr15), indicating increased activation of this kinase, which promotes cell entry into mitosis. This result, together with the evident increase of the cell population in G2/M, allows us to hypothesize that the newly synthesized compounds, as well as SAHA, do not block cell entry into mitosis, but rather interfere with the subsequent steps of cell division. This hypothesis is further supported by literature data showing the ability of HDACis to disrupt the spindle assembly checkpoint (SAC), a critical cellular mechanism that ensures proper segregation of chromosomes during mitosis. Disruption of this checkpoint can lead to aberrant mitosis and mitotic slippage [50,51]. Overall, these findings provide valuable insights into the therapeutic potential of novel HDACis for glioblastoma treatment. The cell line specific responses highlight the relevance of HDAC isoform expression in determining drug sensitivity, suggesting a possible path toward personalized therapeutic approaches. Moreover, the ability of the new compounds to induce cell cycle arrest and interfere with mitotic progression underscores their potential not only as antiproliferative agents but also as modulators of mitotic integrity, a property that could be exploited to enhance the effectiveness of existing chemotherapeutic strategies.

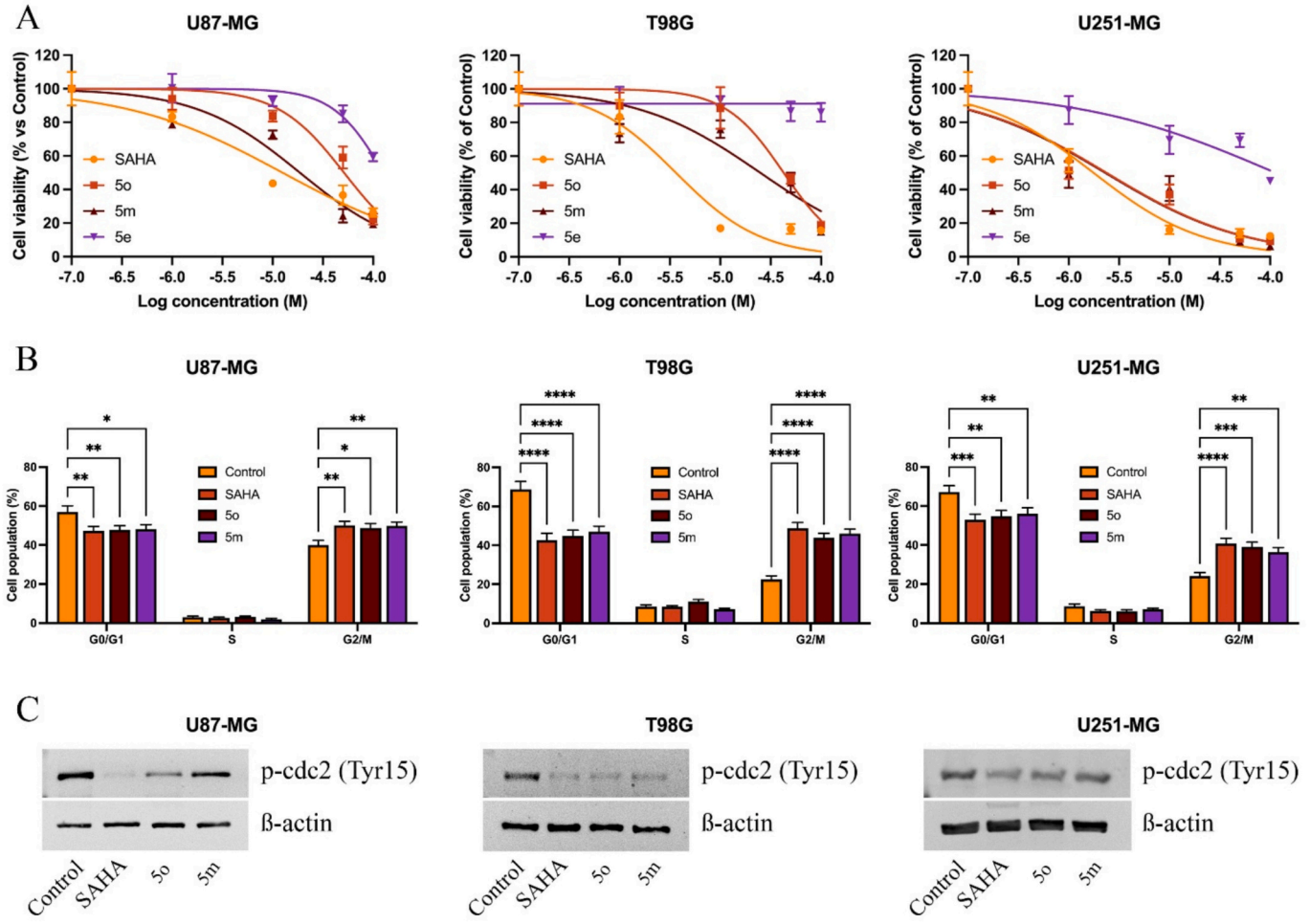

Fig. 8. (**A**) Cell viability assessment of glioblastoma cell lines exposed for 72 h to increasing concentrations (0.1 to 100 μM) of **SAHA**, **5o**, **5m** and **5e**. (**B**) Cell cycle analysis performed on glioblastoma cells treated for 24 h with **SAHA**, **5o** and **5m** (at IC_{50} value calculated at 72 h). (**C**) Immunoblot analysis of p-cdc2 (Tyr15) carried out on glioblastoma cells treated for 24 h with **SAHA**, **5o** and **5 m** (at IC_{50} value calculated at 72 h). Data are presented as mean ± SEM from n = 3 independent experiments. Statistical significance was assessed by two-way ANOVA followed by Dunnett's multiple comparisons test *, $p < 0.05$, **, $p < 0.01$, ***, $p < 0.001$ and ****, $p < 0.0001$ vs control.

2.8. Prediction of Blood Brain Barrier (BBB) permeability for compound 5o

In order to provide an estimation of the BBB penetration for compound **5o**, we employed the deep learning-based pharmacokinetics predictor Deep-PK [52], which has demonstrated to have fair accuracy in predicting ADMET properties. This in silico approach, which relies on graph neural networks, was used to predict the BBB penetration for **5o** in comparison to SAHA and panobinostat, which have been investigated for the treatment of gliomas [53–56]. Deep-PK identified SAHA and panobinostat as BBB-penetrant, and classified **5o** as a compound with BBB permeability (**Fig. S3**).

3. Conclusion

We have developed a novel series of hydroxamic acid-based HDACis inspired by natural vanilloyl and feruloyl motifs. Among these, compound **5o** emerged as a highly potent HDAC6 inhibitor, demonstrating nanomolar activity in vitro and robust cellular target engagement. Its ability to induce α-tubulin acetylation, promote apoptotic pathways in neuroblastoma cells, and impair cell cycle progression in glioblastoma models, highlights its promising therapeutic potential. Importantly, **5o** exhibited minimal cytotoxicity in non-tumoral cells, supporting a favorable safety profile. These findings provide compelling evidence for the utility of vanilloyl-derived scaffolds in the design of HDAC inhibitors and lay the groundwork for further investigations of **5o** as an epigenetic modulator in aggressive neural tumors.

4. Experimental section

4.1. General chemistry information

All reagents were purchased from commercial suppliers and used without further purification. All moisture-sensitive reactions were performed under nitrogen atmosphere using oven-dried glassware and anhydrous solvents. Flash column chromatography was carried out on silica gel (Merck: Kieselgel 60, particle size 0.040–0.063 mm). Reactions' progression was monitored by thin-layer chromatography (TLC), carried out using glass-backed plates coated with Merck Kieselgel 60 GF254. Plates were visualized under UV light (at 254 nm). ^{1}H NMR and ^{13}C NMR spectra were recorded on a Varian 300 MHz or Bruker Avance 400 MHz spectrometers using the residual signal of the deuterated solvent as an internal standard. Coupling constants (*J*) are given in Hertz (Hz). Splitting patterns are described as singlet (s), doublet (d), triplet (t), quartet (q), and broad (br); the values of chemical shifts (δ) are given in parts per million (ppm) [57]. Mass spectra were recorded utilizing an electron spray ionization (ESI) Agilent 1100 Series LC/MSD spectrometer. The purity of final products (>95 %) was determined by

an analytical high-performance liquid chromatography (HPLC) Merk Purospher STAR RP-18e (5 μm) LiChroCART 250–4 column (detection at 254 nm; flow rate = 1.0 mL/min; mobile phase A, 0.01 % TFA (*v*/v) in water; mobile B, acetonitrile; gradient, 90/10–10/90 A/B in 20 min). The gradient was optimized based on compound polarity. LC–HRMS analysis was carried out using an UHPLC instrument (Agilent 1290 Infinity II) coupled to a LC/Q-TOF mass spectrometer fitted with an ESI source operating in positive or negative ion mode (Revident, Agilent Technologies, CA, USA). Data were collected and analyzed using the Mass Hunter software provided by the manufacturer.

4.2. General procedure A: Amide formation from acyl chloride

To a suspension of the suitable carboxylic acid (1 mmol, 1 equiv.) in dry DCM (0.85 mL), dry DMF (1 gtt) and $SOCl_2$ (10 mmol, 10 equiv.) were added. The reaction mixture was stirred at 60 °C for 4–16 h, until TLC displayed complete consumption of the starting material. Then, the solvents were removed by rotary evaporation. The oily residue was dissolved in dry DCM (6.5 mL) and a solution of the suitable amine/aniline in dry DCM (1.1 mmol, 1.1 equiv., 6.5 mL) and DIPEA (4 mmol, 4 equiv.) were added. The reaction mixture was stirred at 25 °C for 18 h and then it was diluted with DCM, quenched with a saturated solution of NH_4Cl and extracted with DCM (3 × 20 mL). The collected organic layers were washed with brine (1 × 20 mL), dried over anhydrous Na_2SO_4, filtered, and concentrated under reduced pressure.

4.3. General procedure B: O-acetylation

To a solution of **6** or **12** (5.95 mmol, 1 equiv.) in pyridine (16 mL), Ac_2O (17.84 mmol, 3 equiv.) and DMAP (0.59 mmol, 0.1 equiv.) were added at 25 °C. The reaction mixture was stirred at 25 °C for 16 h. Then, 50 mL of water were added and the mixture was stirred for 20 min. 1 N HCl was added to pH = 2 and the crude was extracted with EtOAc (3 × 20 mL). The combined organic layers were dried over anhydrous Na_2SO_4, filtered and concentrated under reduced pressure.

4.4. General procedure C: Hydroxylaminolysis of methyl esters

To a stirring solution of hydroxylamine hydrochloride (30 mmol, 30 equiv.) in MeOH (15 mL), a methanolic solution of KOH (37 mmol, 37 equiv., 4 mL) was added at 25 °C. After stirring for 10 min, the suspension was filtered and the filtrate was added to a round-bottom flask containing the suitable methyl ester (1 mmol, 1 equiv.). The reaction mixture was stirred at 25 °C for 6–18 h. Then, 6 N HCl was added dropwise to pH = 7 and the solvent was removed under reduced pressure.

4.5. General procedure D: TMSCl-mediated esterification

To a solution of the suitable carboxylic acid (1 mmol, 1 equiv.) in MeOH (4 mL), TMSCl (2.2 mmol, 2.2 equiv.) was added at 25 °C. The reaction mixture was stirred at 25 °C for 18 h. Then, the volatiles were removed under reduced pressure.

4.6. General procedure E: N-alkylation: insertion of the isopropyl moiety

A solution of **21a** or **21b** (0.87 mmol, 1 equiv.) and isopropylamine (2.62 mmol, 3 equiv.) in dry DMF (1 mL) was stirred at 25 °C for 16 h. Then, a saturated solution of NH_4Cl was added to pH = 5 and the crude was extracted with EtOAc (3 × 10 mL). The combined organic layers were washed with a saturated solution of NaCl (3 × 30 mL), and dried over anhydrous Na_2SO_4, filtered and concentrated under reduced pressure.

Methyl 4-(4-hydroxy-3-methoxybenzamido)benzoate (**7a**). Starting from **6** (108 mg, 0.71 mmol) and **17a** (100 mg, 0.60 mmol), compound **7a** was obtained following General Procedure A. The crude was purified by column chromatography on silica gel (eluent PE/EtOAc, 1:0 to 1:1) to afford the title compound as a white solid (50 % yield). ESI-MS *m/z*: 302 $[M + H]^+$, 324 $[M + Na]^+$. ^1H NMR (300 MHz, $CDCl_3$) δ 8.04 (d, J = 8.7 Hz, 2H), 7.72 (d, J = 8.8 Hz, 2H), 7.52 (d, J = 2.0 Hz, 1H), 7.34 (dd, J = 8.2, 2.0 Hz, 1H), 6.96 (d, J = 8.2 Hz, 1H), 6.04 (br, 1H), 3.96 (s, 3H), 3.91 (s, 3H), 1.65 (br, 1H).

Methyl 4-((4-hydroxy-3-methoxybenzamido)methyl)benzoate (**7b**). Starting from **6** (94 mg, 0.56 mmol) and **20a** (102 mg, 0.62 mmol), compound **7b** was obtained following general procedure A. The crude was purified by column chromatography on silica gel (PE/EtOAc, 3:1 to 1:1) to afford the title compound as a white solid (48 % yield). ESI-MS *m/z*: 316 $[M + H]^+$. ^1H NMR (300 MHz, acetone-d_6) δ 8.35 (d, J = 17.3 Hz, 2H), 7.56 (d, J = 21.8 Hz, 2H), 7.48–7.39 (m, 2H), 6.93–6.83 (m, 1H), 4.64 (s, 2H), 3.92 (br, 1H), 3.86 (s, 3H), 3.82 (s, 3H), 3.23 (br, 1H).

Methyl 3-(4-hydroxy-3-methoxybenzamido)benzoate (**8a**). Starting from **6** (100 mg, 0.60 mmol) and **17b** (108 mg, 0.71 mmol), compound **8a** was obtained following general procedure A. Purification by column chromatography on silica gel (PE/EtOAc, 1:0 to 1:1) afforded the title compound as a white solid (56 % yield). ESI-MS *m/z*: 302 $[M + H]^+$, 324 $[M + Na]^+$. ^1H NMR (300 MHz, $CDCl_3$) δ 8.15 (s, 1H), 8.01 (d, J = 8.0 Hz, 1H), 7.78 (d, J = 8.0 Hz, 1H), 7.50 (s, 1H), 7.45–7.32 (m, 2H), 6.93 (d, J = 8.2 Hz, 1H), 6.33 (d, J = 21.2 Hz, 1H), 6.12 (br, 1H), 3.91 (s, 3H), 3.88 (s, 3H).

Methyl 3-((4-hydroxy-3-methoxybenzamido)methyl)benzoate (**8b**). Starting from **6** (79 mg, 0.47 mmol) and **20b** (85 mg, 0.52 mmol), compound **8b** was obtained following general procedure A. The crude was purified by column chromatography on silica gel (PE/EtOAc, 3:1 to 1:1) to afford the title compound as a white solid (51 % yield). ESI-MS *m/z*: 316 $[M + H]^+$. ^1H NMR (300 MHz, $CDCl_3$) δ 8.00 (s, 1H), 7.95 (d, J = 7.7 Hz, 1H), 7.56 (d, J = 7.6 Hz, 1H), 7.49 (d, J = 1.9 Hz, 1H), 7.42 (t, J = 7.7 Hz, 1H), 7.22 (dd, J = 8.2, 1.9 Hz, 1H), 6.90 (d, J = 8.2 Hz, 1H), 6.48 (br, 1H), 5.98 (s, 1H), 4.67 (d, J = 5.8 Hz, 2H), 3.93 (s, 3H), 3.90 (s, 3H).

Methyl 4-((4-hydroxy-N-isopropyl-3-methoxybenzamido)methyl) benzoate (**9a**). Starting from **6** (250 mg, 1.19 mmol) and **22a** (271 mg, 1.31 mmol), compound **9a** was obtained following General Procedure G. The crude was used in the next step without any further purification, yielding the title compound as a white solid (99 % yield). ^1H NMR (300 MHz, $CDCl_3$) δ 8.00 (d, J = 8.3 Hz, 2H), 7.39 (d, J = 4.6 Hz, 2H), 7.12–6.92 (m, 3H), 4.67 (s, 2H), 4.38–4.19 (m, 1H), 3.91 (s, 3H), 3.84 (s, 3H), 2.32 (s, 3H), 1.14 (s, 6H).

Methyl 3-(4-hydroxy-N-isopropyl-3-methoxybenzamido)methyl) benzoate (**9b**). Starting from **6** (250 mg, 1.19 mmol) and **22b** (271 mg, 1.31 mmol), compound **9b** was obtained following General Procedure A. The crude was used in the next step without any further purification, yielding the title compound as a white solid (89 % yield). ^1H NMR (300 MHz, $CDCl_3$) δ 7.87 (d, J = 7.7 Hz, 1H), 7.74 (s, 1H), 7.36–7.23 (m, 1H), 7.17 (d, J = 7.8 Hz, 1H), 6.86 (s, 1H), 6.70 (d, J = 8.2 Hz, 1H), 6.58 (d, J = 8.2 Hz, 1H), 5.89 (s, 1H), 5.04 (dt, J = 13.3, 6.8 Hz, 1H), 3.89 (s, 3H), 3.69 (s, 3H), 1.20 (d, J = 6.2 Hz, 6H).

4-Acetoxy-3-methoxybenzoic acid (**10**). Starting from **6** (1000 mg, 5.95 mmol), compound **10** was obtained following general procedure B. The crude was used in the next step without any further purification (99 % yield). ^1H NMR (300 MHz, $CDCl_3$) δ 11.11 (br, 1H), 7.76 (dd, J = 8.2, 1.9 Hz, 1H), 7.71 (d, J = 1.9 Hz, 1H), 7.14 (d, J = 8.2 Hz, 1H), 3.91 (s, 3H), 2.34 (s, 3H).

Methyl 4-((4-acetoxy-N-isopropyl-3-methoxybenzamido)methyl) benzoate (**11a**). Starting from **9** (200 mg, 0.95 mmol) and **18a** (202 mg,1.05 mmol), compound **11a** was obtained following General Procedure A. The crude was purified by column chromatography on silica gel (PE/EtOAc, 1:0 to 1:1) to afford the title compound as a white solid (70 % yield). ^1H NMR (300 MHz, $CDCl_3$) δ 7.91 (d, J = 7.8 Hz, 2H), 7.08 (d, J = 7.9 Hz, 2H), 6.86 (s, 1H), 6.72 (d, J = 7.6 Hz, 1H), 6.59 (d, J = 8.2 Hz, 1H), 5.80 (s, 1H), 5.13–4.95 (m, 1H), 3.88 (s, 3H), 3.70 (s, 3H), 2.29 (s, 3H), 1.22 (d, J = 6.7 Hz, 6H).

Methyl 3-((4-acetoxy-N-isopropyl-3-methoxybenzamido)methyl) benzoate (**11b**). Starting from **9** (200 mg, 0.95 mmol) and **18b** (202 mg,1.05 mmol), compound **11b** was obtained following General Procedure A. The crude was purified by column chromatography on silica gel (PE/EtOAc 1:0 to 2:1) to afford the title compound as a white solid (56 % yield). ^{1}H NMR (300 MHz, $CDCl_3$) δ 7.99 (s, 1H), 7.92 (d, $J = 7.5$ Hz, 1H), 7.60–7.46 (m, 1H), 7.40 (t, $J = 7.7$ Hz, 1H), 7.12–6.96 (m, 3H), 4.66 (s, 2H), 4.26 (br, 1H), 3.91 (s, 3H), 3.84 (s, 3H), 2.31 (s, 3H), 1.16 (s, 6H).

trans Methyl-4-(3-(4-hydroxy-3-methoxyphenyl)-N-isopropylacrylamido)benzoate (**14a**). Starting from **13** (100 mg, 0.42 mmol) and **18a** (82 mg, 0.42 mmol), compound **14a** was obtained following general procedure A. The crude was purified by column chromatography on silica gel (PE/EtOAc, 1:1 to 0:1) to afford the title compound as a white solid (53 % yield). ESI-MS *m/z*: 412 $[M + H]^+$. ^{1}H NMR (300 MHz, $CDCl_3$) δ 8.15–7.98 (m, 2H), 7.56 (d, $J = 15.4$ Hz, 1H), 7.20 (d, $J = 8.1$ Hz, 2H), 6.93–6.69 (m, 3H), 5.92 (d, $J = 15.4$ Hz, 1H), 5.16–4.96 (m, 1H), 3.90 (s, 3H), 3.80 (s, 3H), 2.21 (s, 3H), 1.09 (d, $J = 6.8$ Hz, 6H).

trans Methyl-4-(3-(4-acetoxy-3-methoxyphenyl)acrylamido)benzoate (**14b**). Starting from **13** (110 mg, 0.46 mmol) and **17a** (70 mg, 0.46 mmol), compound **14b** was obtained following general procedure A. The crude was purified by column chromatography on silica gel (PE/EtOAc, 1:1 to 0:1) to afford the title compound as a white solid (63 % yield). ESI-MS *m/z*: 368 $[M-H]^-$. ^{1}H NMR (300 MHz, $CDCl_3$) δ 8.03–7.81 (m, 2H), 7.85–7.63 (m, 1H), 7.67–7.36 (m, 2H), 7.29–6.84 (m, 4H), 6.74–6.41 (m, 1H), 3.99–3.51 (m, 6H), 2.27 (s, 3H).

trans Methyl-4-((3-(4-acetoxy-3-methoxyphenyl)-N-isopropylacrylamido)methyl)benzoate (**14c**). Starting from **13** (132 mg, 0.56 mmol) and **22a** (116 mg, 0.56 mmol), compound **14c** was obtained following general procedure A. The crude was purified by column chromatography on silica gel (PE/EtOAc, 1:1 to 0:1) to afford the title compound as a white solid (47 % yield). ESI-MS *m/z*: 426 $[M + H]^+$. ^{1}H NMR (300 MHz, acetone-d_6) δ 8.13–7.80 (m, 2H), 7.64 (d, $J = 15.0$ Hz, 1H), 7.57–7.20 (m, 4H), 7.23–6.69 (m, 2H), 4.79 (d, $J = 28.4$ Hz, 2H), 3.86 (s, 7H), 2.26–2.16 (m, 3H), 1.16 (s, 6H).

***trans Methyl-4-((3-(4-hydroxy-3-methoxyphenyl)acrylamido)methyl)benzoate (*14d**). Starting from *trans* ferulic acid **12** (107 mg, 0.55 mmol) and **20a** (100 mg, 0.55 mmol), compound **14d** was obtained following general procedure A. The crude was purified by column chromatography on silica gel (PE/EtOAc, 1:1 to 0:1) to afford the title compound as a white solid (53 % yield). ESI-MS *m/z*: 342 $[M + H]^+$. ^{1}H NMR (300 MHz, $CDCl_3$) δ 7.94 (d, $J = 8.2$ Hz, 2H), 7.57 (d, $J = 15.5$ Hz, 1H), 7.32 (d, $J = 8.2$ Hz, 2H), 7.09–6.96 (m, 2H), 6.92 (t, $J = 2.9$ Hz, 1H), 6.85 (d, $J = 8.2$ Hz, 1H), 6.45 (t, $J = 5.8$ Hz, 1H), 6.33 (d, $J = 15.5$ Hz, 1H), 4.57 (d, $J = 5.9$ Hz, 2H), 3.87 (s, 3H), 3.82 (s, 3H).

trans Methyl-3-(3-(4-acetoxy-3-methoxyphenyl)-N-isopropylacrylamido)benzoate (**15a**). Starting from **13** (107 mg, 0.52 mmol) and **18b** (101 mg, 0.52 mmol), compound **15a** was obtained following general procedure A. The crude was purified by column chromatography on silica gel (PE/EtOAc, 1:1 to 0:1) to afford the title compound as a white solid (39 % yield). ESI-MS *m/z*: 412 $[M + H]^+$. ^{1}H NMR (300 MHz, acetone-d_6) δ 8.05–7.80 (m, 3H), 7.70–7.57 (m, 1H), 7.50–7.41 (m, 2H), 7.23–7.09 (m, 1H), 6.90–6.61 (m, 2H), 3.95–3.74 (m, 7H), 2.30 (s, 3H), 1.30–1.10 (m, 6H).

trans Methyl-3-(3-(4-acetoxy-3-methoxyphenyl)acrylamido)benzoate (**15b**). Starting from **13** (136 mg, 0.57 mmol) and **17b** (111 mg, 0.57 mmol), compound **15b** was obtained following general procedure A. The crude was purified by column chromatography on silica gel (PE/EtOAc 1:1) to afford the title compound as a white solid (57 % yield). ESI-MS *m/z*: 368 $[M-H]^-$. ^{1}H NMR (300 MHz, $CDCl_3$) δ 8.30 (d, $J = 13.5$ Hz, 1H), 8.17 (t, $J = 1.9$ Hz, 1H), 8.08–7.94 (m, 1H), 7.84–7.57 (m, 2H), 7.36 (td, $J = 8.0$, 1.4 Hz, 1H), 7.08–6.76 (m, 3H), 6.47 (d, $J = 15.4$ Hz, 1H), 3.91–3.73 (m, 6H), 3.49 (s, 1H), 2.23 (s, 3H).

trans Methyl-3-((3-(4-acetoxy-3-methoxyphenyl)-N-isopropylacrylamido)methyl)benzoate (**15c**). Starting from **13** (95 mg, 0.40 mmol) and **22b** (83 mg, 0.40 mmol), compound **15c** was obtained following general procedure A. The crude was purified by column chromatography on silica gel (PE/EtOAc 1:1) to afford the title compound as a yellow solid (24 % yield). ESI-MS *m/z*: 426 $[M + H]^+$, 448 $[M+ Na]^+$. ^{1}H NMR (300 MHz, $CDCl_3$) δ 7.96–7.73 (m, 2H), 7.61 (d, $J = 15.1$ Hz, 1H), 7.50–7.17 (m, 2H), 7.18–6.64 (m, 4H), 4.60 (d, $J = 6.8$ Hz, 2H), 3.86–3.57 (m, 7H), 2.21 (s, 3H), 1.23–0.96 (m, 6H).

trans Methyl-3-((3-(4-hydroxy-3-methoxyphenyl)acrylamido)methyl)benzoate (**15d**). Starting from **13** (98 mg, 0.41 mmol) and **20b** (69 mg, 0.41 mmol), compound **15d** was obtained following general procedure A. The crude was purified by column chromatography on silica gel (PE/EtOAc 1:1) to afford the title compound as a yellow solid (37 % yield). ESI-MS *m/z*: 341 $[M-H]^-$. ^{1}H NMR (300 MHz, acetone-d_6) δ 8.13–7.67 (m, 3H), 7.67–7.52 (m, 1H), 7.50–7.32 (m, 2H), 7.26–7.10 (m, 1H), 6.90–6.74 (m, 1H), 6.60 (dd, $J = 15.7$, 8.7 Hz, 1H), 4.59 (d, $J = 5.9$ Hz, 2H), 4.01–3.74 (m, 7H), 2.86 (s, 1H).

Methyl 4-a*mino*benzoate (**17a**). Starting from 4-aminobenzoic acid **16a** (1000 mg, 7.29 mmol), compound **17a** was obtained following general procedure D. The solid residue was treated with a saturated solution of $NaHCO_3$ (10 mL) and extracted with DCM (3 × 10 mL). The combined organic layers were dried over anhydrous Na_2SO_4, filtered, and concentrated under reduced pressure. The product was used in the next step without further purification (99 % yield, white solid). ESI-MS *m/z*: 174 $[M + Na]^+$. ^{1}H NMR (300 MHz, CD_3OD) δ 8.17 (d, $J = 8.7$ Hz, 2H), 7.49 (d, $J = 8.4$ Hz, 2H), 3.94 (s, 3H).

Methyl 3-aminobenzoate (**17b**). Starting from 3-aminobenzoic acid **16a** (1000 mg, 7.29 mmol), compound **17b** was obtained following general procedure D. The solid residue was treated with a saturated solution of $NaHCO_3$ (10 mL) and extracted with DCM (3 × 10 mL). The combined organic layers were dried over anhydrous Na_2SO_4, filtered and concentrated under reduced pressure. The product was used in the next step without further purification (99 % yield, white solid). ESI-MS *m/z*: 174 $[M + Na]^+$. ^{1}H NMR (300 MHz, CD_3OD) δ 8.17–8.03 (m, 2H), 7.74–7.65 (m, 2H), 3.94 (d, $J = 1.1$ Hz, 3H).

Methyl 4-(isopropylamino)benzoate (**18a**). To a solution of **17a** (300 mg, 1.99 mmol) and acetone (162 μL, 2.18 mmol) in DMF, TMSCl (630 μL, 4.96 mmol) was added at 25 °C. The reaction mixture was cooled to 0 °C, and $NaBH_4$ (75 mg, 4.99 mmol) was added in one solution. The mixture was stirred at 0 °C for 20 min. Then, a saturated solution of $NaHCO_3$ was added to pH = 8 and the crude was extracted with EtOAc (3 × 10 mL). The combined organic layers were washed with a saturated solution of NaCl (3 × 30 mL), and dried over anhydrous Na_2SO_4, filtered and concentrated under reduced pressure. The crude was used in the next step without any further purification (99 % yield). ESI-MS *m/z*: 216 $[M + Na]^+$. ^{1}H NMR (300 MHz, $CDCl_3$) δ 7.90 (d, $J = 8.2$ Hz, 2H), 7.27 (d, $J = 10.1$ Hz, 2H), 5.44 (t, $J = 5.7$ Hz, 1H), 4.37 (d, $J = 5.6$ Hz, 1H), 3.85 (s, 3H), 3.36 (t, $J = 5.0$ Hz, 3H), 2.36 (t, $J = 5.0$ Hz, 3H).

Methyl 3-(isopropylamino)benzoate (**18b**). Compound **18b** was obtained from **17b** (300 mg, 1.99 mmol), by following the same procedure described for **17a**. The crude was used in the next step without any further purification (99 % yield). ESI-MS *m/z*: 216 $[M + Na]^+$. ^{1}H NMR (300 MHz, $CDCl_3$) δ 7.33 (dt, $J = 7.7$, 1.3 Hz, 1H), 7.25 (dd, $J = 2.6$, 1.6 Hz, 1H), 7.19 (t, $J = 7.8$ Hz, 1H), 6.73 (ddd, $J = 8.1$, 2.6, 1.1 Hz, 1H), 3.87 (s, 3H), 3.75–3.56 (m, 1H), 1.19 (d, $J = 6.3$ Hz, 6H).

Methyl 4-(aminomethyl)benzoate hydrochloride (**20a**). Starting from (4-aminomethyl)benzoic acid **19a** (200 mg, 1.32 mmol), compound **20a** was obtained following general procedure D. The product was used in the next step without further purification (99 % yield, white powder). ESI-MS *m/z*: 166 $[M + H]^+$, 188 $[M + Na]^+$. ^{1}H NMR (300 MHz, CD_3OD) δ 8.07 (d, $J = 7.7$ Hz, 2H), 7.61 (d, $J = 8.0$ Hz, 2H), 4.22 (s, 2H), 3.91 (s, 3H), 1.29 (d, $J = 5.1$ Hz, 1H).

Methyl 3-(aminomethyl)benzoate hydrochloride (**20b**). To a solution of methyl 3-cyanobenzoate **19b** (157 mg, 0.97 mmol) in MeOH (4 mL), 12 N HCl (118 μL, 1.42 mmol) and 10 % Pd/C (16 mg) were added at 25 °C. The reaction mixture was stirred under an H_2 atmosphere for 3 h. Then, the catalyst was filtered off and the volatiles were removed

under reduced pressure. The product was used in the next step without further purification (99 % yield, white powder). ESI-MS *m/z*: 166 $[M + H]^+$. ^{1}H NMR (300 MHz, CD_3OD) δ 7.98 (s, 1H), 7.90 (m, 1H), 7.50 (m, 1H), 7.40 (t, $J = 7.8$ Hz, 1H), 4.09 (s, 2H), 3.90 (s, 3H).

Methyl 4-((isopropylamino)methyl)benzoate (**22a**). Starting from **21a** (200 mg, 0.87 mmol), compound **22a** was obtained following general procedure E. The crude was used in the next step without any further purification (89 % yield, white solid). ^{1}H NMR (300 MHz, $CDCl_3$) δ 7.98 (d, $J = 7.7$ Hz, 2H), 7.38 (d, $J = 7.8$ Hz, 2H), 3.89 (s, 3H), 3.83 (s, 2H), 2.84 (p, $J = 6.7$, 6.2 Hz, 1H), 1.25 (s, 1H), 1.09 (s, 6H).

Methyl 3-((isopropylamino)methyl)benzoate (**22b**). Starting from **21b** (1000 mg, 7.29 mmol), compound **22b** was obtained following general procedure E. The product was used in the next step without further purification (82 % yield, white solid). ^{1}H NMR (300 MHz, $CDCl_3$) δ 7.96 (s, 1H), 7.89 (dt, $J = 7.7$, 1.5 Hz, 1H), 7.51 (dt, $J = 7.9$, 1.6 Hz, 1H), 7.36 (t, $J = 7.6$ Hz, 1H), 3.88 (s, 3H), 3.80 (s, 2H), 2.91–2.73 (m, 1H), 1.57 (s, 1H), 1.07 (d, $J = 6.2$ Hz, 6H).

Methyl 4-(N-isopropyl-3,5-bis(trifluoromethyl)benzamido)benzoate (**24**). To a solution of **A** (100 mg, 0.39 mmol) in dry DCM (2 mL), $(COCl)_2$ (37 μL, 0.43 mmol) and 1 gtt. of DMF were added at rt., under N_2. The reaction mixture was stirred at rt. for 2 h. DMF was added to quench the excess of $(COCl)_2$ and then, the solvent was removed under reduced pressure. The residue was dissolved in DCM (1 mL) and a solution of **18a** (75 mg, 0.39 mmol) and DIPEA (337 μL, 1.93 mmol) in DMF (1 mL) was added at rt. The reaction mixture was stirred at rt. for 16 h. Then, it was diluted with DCM, treated with a saturated solution of NH_4Cl and extracted with DCM (3 × 10 mL). The collected organic layers were washed with brine (2 × 10 mL), dried over sodium sulphate, filtered, and concentrated. The crude was used in the next step without any further purification (56 % yield). ESI-MS *m/z*: 434 $[M + H]^+$.

N-(4-(Hydroxycarbamoyl)phenyl)-N-isopropyl-3,5-bis(trifluoromethyl)benzamide (**4**). Starting from **24** (94 mg, 0.22 mmol), compound **4** was obtained following General Procedure C. The crude was purified by column chromatography on silica gel (12:1 $CHCl_3$/MeOH) to afford the title compound as a light-brown solid (55 % yield). ^{1}H NMR (400 MHz, CD_3OD) δ 7.82 (d, $J = 12.8$ Hz, 3H), 7.67 (d, $J = 8.0$ Hz, 2H), 7.31 (d, $J = 7.9$ Hz, 2H), 5.04–4.98 (m, 1H), 1.24 (d, $J = 6.7$ Hz, 6H). ^{13}C NMR (101 MHz, CD_3OD) δ 167.7, 165.2, 141.5, 139.2, 131.4, 130.5, 128.3, 127.6, 124.2, 122.3, 121.5, 48.8, 19.6. ^{19}F NMR (376 MHz, CD_3OD) δ −64.5 (s, 6F). ESI-MS *m/z* 435 $[M + H]^+$. HRMS (ESI) *m/z* $[M + H]^+$ calcd for $C_{19}H_{17}F_6N_2O_3$ 435.1138, found 435.1443. Spectroscopic data are in agreement with those reported by Gunning et al. [26] in *J. Med. Chem. 2020, 63, 8634–8648*. Literature data: ^{1}H NMR (700 MHz, CD_3OD): δ 7.85 (s, 2H), 7.80 (s, 1H), 7.70 (d, $J = 8.2$ Hz, 2H), 7.33 (d, $J = 8.2$ Hz, 2H), 5.02 (br, 1H), 1.24 (d, $J = 7.1$ Hz, 6H). ^{13}C NMR (176 MHz, CD_3OD) δ 170.33, 167.87, 144.15, 141.90, 134.70, 133.60, 133.47, 131.00, 130.29, 125.53, 125.06, 51.38, 22.32. ^{19}F NMR (658 MHz, CD_3OD) δ −64.52 (s, 6F).

4-Hydroxy-N-(4-(hydroxycarbamoyl)phenyl)-N-isopropyl-3-methoxybenzamide (**5a**). Starting from **10a** (62 mg, 0.16 mmol), compound **5a** was obtained following General Procedure C. The crude was purified by column chromatography on silica gel ($CHCl_3$/MeOH, 10:1 to 8:1) to afford the title compound as a light-brown solid (68 % yield). ^{1}H NMR (400 MHz, DMSO-d_6) δ 11.16 (s, 1H), 9.25 (s, 1H), 8.98 (s, 1H), 7.61 (d, $J = 8.4$ Hz, 2H), 7.16 (d, $J = 8.4$ Hz, 2H), 6.73–6.64 (m, 2H), 6.50 (d, $J = 8.1$ Hz, 1H), 4.80 (p, $J = 6.7$ Hz, 1H), 3.50 (s, 3H), 1.09 (d, $J = 6.8$ Hz, 6H). ^{13}C NMR (101 MHz, DMSO-d_6) δ 169.5, 163.9, 148.0, 146.8, 143.4, 131.5, 130.8, 128.0, 127.7, 122.4, 114.9, 113.2, 55.8, 48.1, 21.2. HRMS (ESI) *m/z* $[M + H]^+$ calcd for $C_{18}H_{21}N_2O_5$ 345.1445, found 345.1445, $[M + Na]^+$ calcd for $C_{18}H_{20}N_2O_5Na$ 367.1264, found 367.1265.

4-Hydroxy-N-(3-(hydroxycarbamoyl)phenyl)-N-isopropyl-3-methoxybenzamide (**5b**). Starting from **11a** (31 mg, 0.08 mmol), compound **5b** was obtained following General Procedure C. The crude was purified by column chromatography on silica gel ($CHCl_3$/MeOH,10:1) to afford the title compound as a light-brown solid (46 % yield). ^{1}H NMR (400 MHz, CD_3OD) δ 7.95–7.86 (m, 1H), 7.77 (s, 1H), 7.32 (t, $J = 7.7$ Hz, 1H), 7.20 (d, $J = 7.5$ Hz, 1H), 6.84–6.76 (m, 2H), 6.56 (d, $J = 8.1$ Hz, 1H), 5.04–4.96 (m, 1H), 3.64 (s, 3H), 1.25 (d, $J = 6.8$ Hz, 6H). ^{13}C NMR (101 MHz, CD_3OD) δ 171.3, 169.3, 147.7, 146.5, 139.9, 137.9, 132.5, 131.1, 128.2, 127.9, 127.6, 122.1, 113.9, 112.1, 54.6, 20.7. HRMS (ESI) *m/z* $[M + H]^+$ calcd for $C_{18}H_{21}N_2O_5$ 345.1445, found 345.1447, $[M + Na]^+$ calcd for $C_{18}H_{20}N_2O_5Na$ 367.1264, found 367.1265.

4-Hydroxy-N-(4-(hydroxycarbamoyl)phenyl)-3-methoxybenzamide (**5c**). Starting from **7a** (33 mg, 0.11 mmol), compound **5c** was obtained following General Procedure C. The crude was purified by column chromatography on silica gel ($CHCl_3$/MeOH, 30:1 to 20:1) to afford the title compound as a brownish green solid (51 % yield). ^{1}H NMR (300 MHz, CD_3OD) δ 7.87–7.73 (m, 4H), 7.58–7.46 (m, 2H), 6.89 (d, $J = 8.2$ Hz, 1H), 3.94 (s, 3H). ^{13}C NMR (75 MHz, CD_3OD) δ 167.4, 150.5, 147.5, 142.3, 130.2, 127.5, 125.5, 121.3, 120.0, 119.7, 114.5, 110.9, 55.1. ESI-MS *m/z*: 301 $[M-H]^-$. HRMS (ESI) *m/z* $[M + H]^+$ calcd for $C_{15}H_{15}N_2O_5$ 303.0975, found 303.0982, $[M + Na]^+$ calcd for $C_{15}H_{14}N_2O_5Na$ 325.0795, found 325.0795.

4-Hydroxy-N-(3-(hydroxycarbamoyl)phenyl)-3-methoxybenzamide (**5d**). Starting from **8a** (246 mg, 0.82 mmol), compound **5d** was obtained following General Procedure C. The crude was purified by column chromatography on silica gel (DCM/MeOH/NH_4OH, 10:1:0.1 to 5:1:0.1) to afford the title compound as a reddish brown solid (68 % yield). ^{1}H NMR (400 MHz, CD_3OD) δ 8.10 (s, 1H), 7.88 (dd, $J = 8.1$, 2.2 Hz, 1H), 7.73 (d, $J = 7.7$ Hz, 1H), 7.57 (s, 1H), 7.51 (dd, $J = 8.3$, 2.0 Hz, 1H), 7.38 (t, $J = 7.9$ Hz, 1H), 6.90 (d, $J = 8.2$ Hz, 1H), 3.94 (s, 3H). ^{13}C NMR (101 MHz, CD_3OD) δ 172.8, 167.2, 150.2, 147.5, 138.3, 136.9, 127.9, 125.8, 124.9, 123.5, 121.8, 121.1, 115.4, 110.9, 55.1. ESI-MS *m/z*: 301 $[M-H]^-$.

***trans N*-hydroxy-4-(3-(4-hydroxy-3-methoxyphenyl)-*N*-isopropylacrylamido)benzamide** (**5e**). Starting from **14a** (200 mg, 0.49 mmol), compound **5e** was obtained following General Procedure C. The crude was purified by column chromatography on silica gel (DCM/MeOH/NH_4OH, 10:1:0.1 to 5:1:0.1) to afford the title compound as a brown solid (28 % yield). ^{1}H NMR (400 MHz, CD_3OD) δ 7.86 (d, $J = 7.2$ Hz, 2H), 7.46–7.31 (m, 3H), 6.87–6.54 (m, 3H), 5.89 (s, 1H), 4.98 (s, 1H), 3.72 (s, 3H), 1.11 (s, 6H). ^{13}C NMR (101 MHz, CD_3OD) δ 166.5, 165.8, 148.6, 147.7, 142.3, 141.2, 132.4, 130.6, 127.8, 126.7, 121.3, 115.9, 115.0, 110.7, 54.9, 46.94, 19.8. ESI-MS *m/z*: 371 $[M + H]^+$. HRMS (ESI) *m/z* $[M + H]^+$ calcd for $C_{20}H_{23}N_2O_5$ 371.1601, found 371.1605, $[M + Na]^+$ calcd for $C_{20}H_{22}N_2O_5Na$ 393.1421, found 393.1423.

trans N-Hydroxy-3-(3-(4-hydroxy-3-methoxyphenyl)-N-isopropylacrylamido)benzamide (**5f**). Starting from **15a** (175 mg, 0.42 mmol), compound **5f** was obtained following General Procedure C. The crude was purified by column chromatography on silica gel (DCM/MeOH/NH_4OH, 10:1:0.1 to 5:1:0.1) to afford the title compound as a brown solid (31 % yield). ^{1}H NMR (400 MHz, CD_3OD) δ 7.73–7.58 (m, 2H), 7.58–7.38 (m, 2H), 6.93–6.55 (m, 3H), 5.92 (d, $J = 15.4$ Hz, 1H), 5.14–4.93 (m, 1H), 3.91 (s, 1H), 3.77 (s, 4H), 1.40–1.27 (m, 2H), 1.21–1.11 (m, 6H). ^{13}C NMR (101 MHz, CD_3OD) δ 166.7, 165.4, 148.6, 147.7, 145.5, 142.35, 138.6, 134.8, 133.6, 129.4, 126.8, 122.5, 121.3, 115.9, 114.4, 110.7, 110.3, 54.8, 22.7, 19.9. ESI-MS *m/z*: 371 $[M + H]^+$. HRMS (ESI) *m/z* $[M + H]^+$ calcd for $C_{20}H_{23}N_2O_5$ 371.1601, found 371.1632, $[M + Na]^+$ calcd for $C_{18}H_{20}N_2O_5Na$ 393.1421, found 393.1426.

trans N-hydroxy-4-(3-(4-hydroxy-3-methoxyphenyl)acrylamido)benzamide (**5g**). Starting from **14b** (146 mg, 0.39 mmol), compound **5g** was obtained following General Procedure C. The crude was purified by column chromatography on silica gel (DCM/MeOH/NH_4OH, 10:1:0.1 to 5:1:0.1) to afford the title compound as a brown solid (21 % yield). ^{1}H NMR (300 MHz, DMSO-d_6) δ 9.39 (s, 1H), 9.19–8.81 (m, 2H), 7.54–7.17 (m, 1H), 7.25–6.89 (m, 3H), 6.77 (d, $J = 8.1$ Hz, 1H), 6.26 (d, $J = 15.7$ Hz, 1H), 3.78 (s, 3H). ^{13}C NMR (101 MHz, CD_3OD) δ 165.6, 148.8, 148.5, 147.8, 140.6, 128.2, 126.7, 122.3, 121.7, 115.5, 115.0, 113.7, 113.4, 110.2, 55.0. ESI-MS *m/z*: 327 $[M-H]^-$. HRMS (ESI) *m/z* [M +

Na]$^+$ calcd for $C_{17}H_{16}N_2O_5Na$ 351.0951, found 351.0951.

trans N-hydroxy-3-(3-(4-hydroxy-3-methoxyphenyl)acrylamido) benzamide (**5h**). Starting from **15b** (191 mg, 0.51 mmol), compound **5h** was obtained following General Procedure C. The crude was purified by column chromatography on silica gel (DCM/MeOH/NH_4OH, 10:1:0.1 to 5:1:0.1) to afford the title compound as a brown solid (21 % yield). ^1H NMR (300 MHz, DMSO-d_6) δ 8.05 (s, 1H), 7.83 (d, J = 6.6 Hz, 1H), 7.61–7.27 (m, 4H), 7.18 (d, J = 1.9 Hz, 1H), 7.12–6.94 (m, 1H), 6.81 (d, J = 8.1 Hz, 1H), 6.62 (d, J = 15.6 Hz, 1H), 3.81 (s, 3H). ^{13}C NMR (75 MHz, DMSO-d_6) δ 170.8, 164.7, 164.5, 149.1, 148.3, 140.1, 134.0, 129.2, 126.5, 122.4, 111.3, 60.2 (2C). ESI-MS *m/z*: 327 [M-H]$^-$. HRMS (ESI) *m/z* [M + H]$^+$ calcd for $C_{17}H_{17}N_2O_5$ 329.1132, found 329.1132, [M + Na]$^+$ calcd for $C_{17}H_{16}N_2O_5Na$ 351.0951, found 351.0950.

4-Hydroxy-N-(4-(hydroxycarbamoyl)benzyl)-N-isopropyl-3-methoxybenzamide (**5i**). Starting from **10b** (475 mg, 1.19 mmol), compound **5i** was obtained following General Procedure C. The crude was purified by column chromatography on silica gel ($CHCl_3$/MeOH, 10:1 to 8:1) to afford the title compound as a light-brown solid (24 % yield). ^1H NMR (400 MHz, DMSO-d_6) δ 11.18 (s, 1H), 9.36 (s, 1H), 9.06 (s, 1H), 7.73 (d, J = 8.2 Hz, 2H), 7.38 (d, J = 8.0 Hz, 2H), 6.96 (s, 1H), 6.93–6.86 (m, 1H), 6.83 (d, J = 8.3 Hz, 1H), 4.57 (s, 2H), 4.20 (br, 1H), 3.75 (s, 3H), 1.10 (d, J = 6.7 Hz, 6H). ^{13}C NMR (101 MHz, DMSO-d_6) δ 171.6, 164.7, 148.1, 147.8, 143.6, 131.4, 128.3, 127.3, 127.0, 119.8, 115.5, 111.2, 56.1, 49.1, 21.1. ESI-MS *m/z*: 359 [M + H]$^+$, 397 [M + K]$^+$. HRMS (ESI) *m/z* [M + H]$^+$ calcd for $C_{19}H_{23}N_2O_5$ 359.1601, found 359.1598,[M + Na]$^+$ calcd for $C_{19}H_{22}N_2O_5Na$ 381.1421, found 381.1420.

4-Hydroxy-N-(3-(hydroxycarbamoyl)benzyl)-N-isopropyl-3-methoxybenzamide (**5j**). Starting from **11b** (415 mg, 1.04 mmol), compound **5j** was obtained following General Procedure C. The crude was purified by column chromatography on silica gel ($CHCl_3$/MeOH, 10:1 to 5:1) to afford the title compound as a light-brown solid (39 % yield). ^1H NMR (400 MHz, CD_3OD) δ 7.76 (s, 1H), 7.62 (d, J = 7.6 Hz, 1H), 7.56–7.51 (m, 1H), 7.49–7.40 (m, 1H), 7.03 (s, 1H), 6.97 (d, J = 8.1 Hz, 1H), 6.88 (m, 1H), 4.70 (s, 2H), 4.38–4.34 (m, 1H), 3.87 (s, 3H), 1.22 (d, J = 4.5 Hz, 6H). ^{13}C NMR (101 MHz, CD_3OD) δ 174.2, 148.9, 148.4, 140.6, 133.1, 131.8, 130.7, 129.1, 128.4, 126.2, 125.8, 120.1, 115.5, 110.8, 57.7, 55.8, 44.0, 20.6. ESI-MS *m/z*: 359 [M + H]$^+$, 397 [M + K]$^+$. HRMS (ESI) *m/z* [M + H]$^+$ calcd for $C_{19}H_{23}N_2O_5$ 359.1601, found 359.1594, [M + Na]$^+$ calcd for $C_{19}H_{22}N_2O_5Na$ 381.1421, found 381.1420.

4-Hydroxy-N-(4-(hydroxycarbamoyl)benzyl)-3-methoxybenzamide (**5k**). Starting from **7b** (85 mg, 0.27 mmol), compound **5k** was obtained following General Procedure C. The crude was purified by column chromatography on silica gel ($CHCl_3$/MeOH 10:1) to afford the title compound as a brown solid (52 % yield). ^1H NMR (300 MHz, CD_3OD) δ 7.71 (d, J = 5.7 Hz, 2H), 7.49–7.35 (m, 4H), 6.83 (d, J = 7.3 Hz, 1H), 4.60 (s, 2H), 3.89 (s, 3H). ^{13}C NMR (75 MHz, CD_3OD) δ 150.0, 147.4, 143.3, 130.7, 127.2, 127.2, 127.0, 126.9, 125.1, 120.7, 114.5, 110.5, 55.1, 42.8. ESI-MS *m/z*: 315 [M-H]$^-$. HRMS (ESI) *m/z* [M + H]$^+$ calcd for $C_{16}H_{17}N_2O_5$ 317.1132, found 317.1133, [M + Na]$^+$ calcd for $C_{16}H_{16}N_2O_5Na$ 339.0951, found 339.0951.

4-Hydroxy-N-(3-(hydroxycarbamoyl)benzyl)-3-methoxybenzamide (**5l**). Starting from **8b** (76 mg, 0.24 mmol), compound **5 l** was obtained following General Procedure C. The crude was purified by column chromatography on silica gel ($CHCl_3$/MeOH 10:1) to afford the title compound as a brown solid (35 % yield). ^1H NMR (300 MHz, CD_3OD) δ 8.85 (s, 1H), 7.73 (s, 1H), 7.61 (d, J = 7.6 Hz, 1H), 7.56–7.45 (m, 2H), 7.41 (dd, J = 8.5, 6.3 Hz, 2H), 6.84 (d, J = 8.0 Hz, 1H), 4.59 (d, J = 3.9 Hz, 2H), 3.89 (s, 3H).^{13}C NMR (75 MHz, CD_3OD) δ 168.5, 166.8, 150.0, 147.4, 139.8, 132.4, 130.4, 128.4, 125.8, 125.4, 125.1, 120.7, 114.5, 110.6, 55.0, 42.8. ESI-MS *m/z*: 315 [M-H]$^-$. HRMS (ESI) *m/z* [M + H]$^+$ calcd for $C_{16}H_{17}N_2O_5$ 317.1132, found 317.1136, [M + Na]$^+$ calcd for $C_{16}H_{16}N_2O_5Na$ 339.0951, found 339.0955.

trans N-hydroxy-4-((3-(4-hydroxy-3-methoxyphenyl)-N-isopropylacrylamido)methyl)benzamide (**5m**). Starting from **14c** (52 mg, 0.12 mmol), compound **5m** was obtained following General Procedure C. The crude was purified by column chromatography on silica gel ($CHCl_3$/MeOH/NH_4OH 10:1:0.1) to afford the title compound as a brown solid (8 % yield). ^1H NMR (300 MHz, DMSO-d_6) δ 11.12 (s, 1H), 9.39 (s, 1H), 8.96 (s, 1H), 7.68 (dd, J = 14.5, 7.8 Hz, 2H), 7.54–6.85 (m, 5H), 6.85–6.48 (m, 2H), 4.66 (d, J = 50.0 Hz, 2H), 3.76 (d, J = 36.9 Hz, 4H), 1.15–1.01 (m, 6H). ^{13}C NMR (75 MHz, DMSO-d_6) δ 166.9, 166.6, 148.8, 148.3, 144.1, 142.7, 127.5, 127.1, 126.6, 122.8, 115.9, 115.6, 111.8, 79.6, 56.2, 48.3, 45.6, 21.9, 20.6. ESI-MS *m/z*: 385 [M + H]$^+$. HRMS (ESI) *m/z* [M + H]$^+$ calcd for $C_{21}H_{25}N_2O_5$ 385.1758, found 385.1764, [M + Na]$^+$ calcd for $C_{21}H_{24}N_2O_5Na$ 407.1577, found 407.1580.

trans N-hydroxy-3-((3-(4-hydroxy-3-methoxyphenyl)-N-isopropylacrylamido)methyl)benzamide (**5n**). Starting from **15c** (25 mg, 0.06 mmol), compound **5n** was obtained following General Procedure C. The crude was purified by column chromatography on silica gel ($CHCl_3$/MeOH/NH_4OH 10:1:0.1) to afford the title compound as a brown solid (8 % yield). ^1H NMR (400 MHz, CD_3OD) δ 7.80–7.16 (m, 6H), 7.15–6.98 (m, 1H), 6.95–6.46 (m, 3H), 4.80–4.44 (m, 3H), 3.97–3.62 (m, 3H), 1.56–0.78 (m, 6H). ^{13}C NMR (101 MHz, CD_3OD) δ 168.7, 166.8, 148.6, 147.9, 144.5, 143.5, 140.2, 132.7, 132.3, 129.8, 129.2, 128.2, 127.1, 125.3, 122.2, 115.3, 115.0, 114.1, 110.5, 55.0, 49.1, 20.4. ESI-MS *m/z*: 385 [M + H]$^+$, 407 [M+ Na]$^+$. HRMS (ESI) *m/z* [M + H]$^+$ calcd for $C_{21}H_{25}N_2O_5$ 385.1758, found 385.1763, [M + Na]$^+$ calcd for $C_{21}H_{24}N_2O_5Na$ 407.1577, found 407.1579.

trans N-Hydroxy-4-((3-(4-hydroxy-3-methoxyphenyl)acrylamido) methyl)benzamide (**5o**). Starting from **14d** (99 mg, 0.29 mmol), compound **5o** was obtained following General Procedure C. The crude was purified by column chromatography on silica gel (DCM/MeOH/NH_4OH 30:1:0 to 10:1:0.1) to afford the title compound as a light-brown solid (35 % yield). ^1H NMR (300 MHz, CD_3OD) δ 7.71 (d, J = 8.0 Hz, 2H), 7.49 (d, J = 15.5 Hz, 1H), 7.39 (d, J = 8.0 Hz, 2H), 7.12 (s, 1H), 7.03 (d, J = 8.1 Hz, 1H), 6.79 (d, J = 8.1 Hz, 1H), 6.50 (d, J = 15.6 Hz, 1H), 4.53 (s, 2H), 3.87 (s, 3H). ^{13}C NMR (75 MHz, CD_3OD) δ 167.8, 166.5, 148.5, 147.9, 142.8, 141.3, 130.9, 127.2, 127.0, 126.7, 121.9, 116.9, 115.0, 110.1, 54.9, 42.4. ESI-MS *m/z*: 341 [M-H]$^-$. HRMS (ESI) *m/z* [M + H]$^+$ calcd for $C_{18}H_{19}N_2O_5$ 343.1288, found 343.1290, [M + Na]$^+$ calcd for $C_{18}H_{18}N_2O_5Na$ 365.1108, found 365.1109.

trans N-Hydroxy-3-((3-(4-hydroxy-3-methoxyphenyl)acrylamido) methyl)benzamide (**5p**). Starting from **15d** (100 mg, 0.29 mmol), compound **5p** was obtained following General Procedure C. The crude was purified by column chromatography on silica gel (DCM/MeOH/NH_4OH 30:1:0.1) to afford the title compound as a light-brown solid (15 % yield). ^1H NMR (400 MHz, CD_3OD) δ 7.76–7.54 (m, 2H), 7.54–7.36 (m, 3H), 7.22–6.93 (m, 4H), 6.78 (dd, J = 8.2, 1.3 Hz, 2H), 6.47 (d, J = 15.6 Hz, 1H), 6.27 (d, J = 15.7 Hz, 1H), 4.51 (s, 2H), 3.29 (s, 3H). ^{13}C NMR (101 MHz, CD_3OD) δ 167.8, 148.5, 147.8, 141.2, 140.6, 139.4, 130.5, 128.5, 126.7, 126.1, 125.8, 125.5, 121.8, 116.9, 115.0, 110.2, 110.1, 54.9. ESI-MS *m/z*: 341 [M-H]$^-$. HRMS (ESI) *m/z* [M + H]$^+$ calcd for $C_{18}H_{19}N_2O_5$ 343.1288, found 343.1292, [M + Na]$^+$ calcd for $C_{18}H_{18}N_2O_5Na$ 365.1108, found 365.1108.

4.7. Docking studies

The X-ray structure of *h*HDAC6 bound to trichostatin A (PDB iD: 5EDU) was used to build a molecular model of the CD2 domain of *h*HDAC6 suitable for docking studies by applying Maestro software [58]. The protein structure was prepared using the Protein Preparation Wizard tool within the Schrödinger 2021–2 suite [59,60]. Following the default procedure, zero-order bonds between the protein and ligand atoms and the Zn^{2+} were created to model the coordination bonds within the catalytic cavity. Hydrogen atoms were added to the structure, and the protonation state of ionizable group was attributed to be consistent with pH 7.4. Histidine and aspartate residues involved in the Zn^{2+} ion chelation (i.e., His651, Asp649 and Asp742) were modelled in their neutral and negatively charged form, respectively. The model was

submitted to energy minimization with OPLS4 force field [59] during which only the hydrogen atoms were left unrestrained. The ligands were built by applying Maestro software, modeling the hydroxamic acid group in its neutral form, and then docked within the binding site of *h*HDAC6 using Glide software [61]. The docking grid was centered on the co-crystallized inhibitor thricostatin A, defining the inner and outer grid edge to 12 and 32 Å, respectively. A metal-coordination restraint between the Zn^{2+} ion and the hydroxamic group was applied. Docking studies were performed using the standard precision (SP) mode, and the docking poses were ranked according to their Gscore value. Only top-ranked poses were considered and discussed here.

4.8. Human HDAC inhibition assays

For the evaluation of their inhibitory activity, different concentrations of the compounds were incubated in a low-binding black 96-well plate with 30 ng of human recombinant HDAC1 (BPS Bioscience; Cat. # 50051), 5 ng of human recombinant HDAC2 (BPS Bioscience; Cat. # 50002), 4 ng of human recombinant HDAC3 (BPS Bioscience; Cat. # 50003), 30 ng of human recombinant HDAC6 (BPS Bioscience, San Diego, CA, USA; Cat. # 50056), 30 ng of human recombinant HDAC8 (BPS Bioscience; Cat. # 50008), or 500 ng of human recombinant HDAC10 (BPS Bioscience; Cat. # 50060) in an assay buffer composed of 25 mM Tris/HCl, pH 8.0, 137 mM NaCl, 2.7 mM KCl, 1 mM $MgCl_2$, and 0.1 mg/mL bovine serum albumin for 30 min at 37 °C. At the end of the incubation, the deacetylation reaction was initiated by adding 200 μM of the fluorogenic acetylated HDAC substrate 3 (BPS Bioscience; Cat. # 50037) for HDAC1, HDAC2, HDAC3 and HDAC10 assays, or of the fluorogenic HDAC substrate class 2 A (BPS Bioscience; Cat. # 50040) for HDAC8 assays. After 30 min at 37 °C, the reaction was stopped by the addition of an HDAC assay developer (BPS Bioscience; Cat. # 50060). Following an incubation of 15 min at RT, fluorescence was measured in an EnSight multimodal plate reader (PerkinElmer, Boston, MA, USA) with an excitation wavelength of 360 nm and an emission wavelength of 450 nm.

4.9. Cell culture

Human SH-SY5Y neuroblastoma cells (ECACC Cat# 94030304, passages 7–20) as well as U87-MG, T98G and U251-MG glioblastoma cells (Cell bank IRCCS AOU San Martino IST (Genova, Italy)), were cultured in Dulbecco's modified Eagle's medium (DMEM), supplemented with 10 % heat-inactivated fetal bovine serum, 100 U mL^{-1} penicillin, and 100 μg mL^{-1} streptomycin. Cell cultures were maintained in a humidified atmosphere at 37 °C and 5 % CO_2.

4.10. Cell Viability

To assess the effects of **5e**, **5 m**, **5o** and SAHA on cell viability, SH-SY5Y and GBM cells were treated with drugs for 24 h, 48 and 72 h and MTT (3-[4,5-dimethylthiazol-2-yl]-2,5-diphenyltetrazolium bromide) assay was performed as already reported [62].

4.11. Cell lysis and protein quantification

Following treatment with the indicated compound at a final concentration of 10 μM, cell were subjected to total and histone protein extraction and quantification as reported. [63]

4.12. Immunoblotting analysis

Equal amounts of protein (30 μg) from total cell lysates were resolved on 10 % SDS–polyacrylamide gels, while 1.5 μg of acid-extracted histone protein were resolved on 10 % SDS–polyacrylamide gels, –while 1.5 μg of acid-extracted histone proteins were separated on 15 % SDS–polyacrylamide gels. Proteins were then transferred onto nitrocellulose membranes via electroblotting. Immunodetection was performed using horseradish peroxidase (HRP)-conjugated secondary antibodies (anti-rabbit, Cat. #1705046; anti-mouse, Cat. #1706516; Bio-Rad), and chemiluminescent signals were obtained by using the Clarity™ Western ECL Substrate (500 mL; Cat. #1705061, Bio-Rad). Primary antibodies included anti-acetylated α-tubulin (Cat. #5335), GAPDH (Cat. #D16H11), H3K9/14 ac (Cat. #7627), and total Histone H4 (Cat. #2592), all from Cell Signaling Technology (Danvers, MA, USA). The anti-acetyl-SMC3 antibody (Cat. #MABE1073) was obtained from Millipore. To assess p-cdc2 levels in glioblastoma cell lysates, Rabbit anti phospho-cdc2 (Tyr15) (10A11) primary antibody (Cell Signaling) was used. Rabbit anti β-actin (13E5) primary antibody (Cell Signaling) was used as loading control. Immunodetection was performed using IRDye® 800CW Goat anti-Rabbit secondary antibodies (LI-COR Biotech), using iBright FL1500 imager (ThermoFisher Scientific). All antibodies were used in accordance with the manufacturers' protocols. Densitometric analysis of immunoreactive bands was carried out using ImageJ software (version 1.44).

4.13. Cell cycle analysis

Flow cytometry was used to investigate whether **5e**, **5m**, **5o** and SAHA could cause loss in DNA, as well as changes in cell cycle progression. SH-SY5Y cells were seeded in a 6-well plate (5×10^5 cells/well) and treated with both compounds at concentrations close to their IC_{50} values for 24 h. Afterward, the cells were treated as previously reported [62]. Red fluorescence (DNA) was detected through a 563–607 nm band-pass filter (FL2 channel, 10^4 cells/sample) using a FACScan flow cytometer (BD Biosciences, San Jose, CA, USA) coupled with Cell Quest software v.3.0, (BD Biosciences, San Jose, CA, USA). The same procedure was applied to assess cell cycle perturbation in GBM cells exposed for 24 h to the different compounds, used at concentrations close to their IC_{50} values (calculated at 72 h).

4.14. Apoptosis detection by flow cytometry

SH-SY5Y cells were seeded in 6-well plates at a density of 2×10^5 cells/well and incubated overnight at 37 °C in a humidified atmosphere with 5 % CO_2. Cells were then treated with compound **5o** (3, 10, or 30 μM) or SAHA (3, 10, or 30 μM) for 24, 48, or 72 h. At the end of the incubation, cells were detached using Accutase (Life Technologies, Monza, Italy), washed twice with cold PBS, and resuspended at a concentration of 1×10^5 cells in 100 μL of Annexin Binding Buffer (Life Technologies). Cells were stained with Annexin V Alexa Fluor™ 488 Ready Flow Conjugate and incubated for 5 min at RT in the dark. Subsequently, 1 μM Sytox™ AADvanced™ Dead Cell Stain was added to the cell suspension. Samples were analyzed using an Attune NxT Flow Cytometer (Thermo Fisher Scientific, Paisley, UK) equipped with a 488 nm excitation laser. Fluorescence emission was collected using a 530/30 bandpass filter for Annexin V Alexa Fluor™ 488 and a 695/40 bandpass filter for Sytox™ AADvanced™. SH-SY5Y cells were gated based on forward and side scatter properties to exclude debris and aggregates. Data were processed to distinguish four cell populations based on Annexin V and SYTOX staining: live cells (Annexin V^-/$Sytox^-$), early apoptotic cells (Annexin V^+/ $Sytox^-$), late apoptotic cells (Annexin V^+/ $Sytox^+$), and necrotic cells (Annexin V^-/$Sytox^+$).

4.15. Caspase-3/7 activity assay

Caspase-3/7 activation was evaluated using a fluorescence-based imaging approach. SH-SY5Y cells were seeded at a density of 2×10^3 cells/well in black, clear-bottom 96-well plates (Greiner Bio-One) in complete medium and incubated overnight at 37 °C in a humidified atmosphere with 5 % CO_2. The following day, cells were treated with compound **5o** or SAHA at concentrations of 3, 10, or 30 μM in a final volume of 200 μL per well and incubated for 24, 48, or 72 h. At the end

of each incubation period, CellEvent™ Caspase-3/7 (Life Technologies) was added to each well. After 30 min of incubation at room temperature in the dark, Hoechst 33342 was added followed by gentle mixing and an additional 30-min incubation. Fluorescence images were acquired using the ImageXpress Pico Automated Cell Imaging System (Molecular Devices).

4.16. Autophagy evaluation: SH-SY5Y cells treatment and Western Blot analysis

For the experiments, cells were seeded in 6-well plates at a density of 0.4×10^6 cells/well. The day after, cells were treated in fresh medium with 3 μM SAHA or 3 μM **5o** for 24 h. Such concentrations were chosen on the basis of the respective IC_{50} values obtained in MTT assay. Both SAHA and compound **5o** were added from 1000 X stock solutions in dimethyl sulfoxide (DMSO) and DMSO alone was used in control samples. The same samples were in parallel co-treated (for the final 6 h) with 30 μM chloroquine (CQ) (Sigma-Aldrich); this lysosomotropic compound, by impairing the fusion of autophagosomes with lysosomes, stalls the autophagic flux at its final step and amplifies LC3-II accumulation [64]. After 24 h of treatment, cells were harvested by trypsinization and resuspended (10^6 cells/100 μL) in ice-cold lysis buffer (20 mM HEPES–NaOH, pH 7.5, containing 10 % sucrose, 0.1 % CHAPS, 0.2 % NP-40, 1 mM EDTA, 5 mM dithiothreitol (DTT), 1 mM phenylmethylsulphonyl fluoride (PMSF), protease and phosphatase inhibitor cocktail (Halt™). After sonication on ice for 6 s (Vibracell, amplitude 60, 25 W) and centrifugation at 19,000*g* for 2 min at 4 °C, the supernatant of cell lysates was assayed for protein concentration by using the Bradford reagent (Biorad). Aliquots of cell lysates (15 μg) were separated by sodium dodecyl sulphate polyacrylamide gel electrophoresis (SDS-PAGE) on Bolt™ Bis-Tris Plus 4–12 % Mini Protein Gels (Invitrogen™) for 35 min at a constant voltage of 200 V. Proteins were electrophoretically transferred to 0.22 μm nitrocellulose membranes with a semidry protein transfer apparatus (Peqlab PerfectBlue™ Semi-Dry Blotter) for 40 min at 12 V. Before adding primary antibodies, quality control and transfer efficiency were assessed by reversible Ponceau S (P7170, Sigma-Aldrich) membrane staining of total proteins. After destaining with 0.01 M NaOH and rinsing with deionized water, nitrocellulose membranes were blocked for 1 h at RT with 10 % skimmed milk in TBS (50 mM Tris, 150 mM NaCl, pH 7.5)/0.05 % Tween 20 (TBST), and probed overnight at 4 °C with the following primary antibodies: anti-LC3A/B (referred to as LC3) (dilution 1:1000; L7543, Sigma-Aldrich) and anti-p62 (dilution 1:500; 5114, Cell Signaling Technologies). Primary antibodies were diluted TBST with 2 % or 5 % bovine serum albumin (BSA), respectively. After three washes with TBST, membranes were incubated for 1 h at RT with anti-rabbit horseradish peroxidase-conjugated secondary antibodies (Sigma-Aldrich), diluted in TBST with 1 % skimmed milk. Proteins were visualized by chemiluminescence (Pierce™ ECL Western Blotting Substrate) with a Alliance Q9-ATOM imaging system (UVITEC, Cambridge, UK) and NineAlliance x64 software (UVITEC). The intensity of protein bands of interest was quantified and normalized by using the total amount of protein of the relative lane, as obtained by Ponceau S membrane staining.

4.17. Statistics

Analysis of data was accomplished using GraphPad Prism version 8.0.2 (GraphPad Software Inc.). Data are reported as mean ± SEM. Statistical analyses and significance were measured by ANOVA and Tukey or Dunnet post-test, as well as with unpaired Student t-test, as appropriate. In all comparisons, $*p < 0.05$ was considered significant.

CRediT authorship contribution statement

Ilaria Cursaro: Writing – original draft, Investigation, Formal analysis. **Luca Frattaruolo:** Writing – original draft, Investigation, Data curation. **Laura Scalvini:** Writing – original draft, Software, Investigation. **Chiara Contri:** Writing – original draft, Investigation, Data curation. **Alessia Bichicchi:** Writing – original draft, Investigation, Data curation. **Nicola Tardiolo:** Writing – original draft, Investigation, Data curation. **Valeria Tudino:** Writing – original draft, Formal analysis, Data curation. **Sara Rossi:** Writing – original draft, Formal analysis, Data curation. **Eugenia Nicol Manti:** Writing – original draft, Formal analysis, Data curation. **Martina Cappello:** Writing – original draft, Formal analysis, Data curation. **Chiara Papulino:** Investigation, Data curation. **Emilia Maellaro:** Writing – original draft, Investigation. **Paola Marcolongo:** Writing – original draft, Investigation. **Rosaria Benedetti:** Writing – original draft, Investigation, Data curation. **Lucia Altucci:** Writing – original draft, Data curation. **Katia Varani:** Validation, Formal analysis. **Marco Mor:** Software, Data curation. **Maria Frosini:** Investigation, Formal analysis, Data curation. **Fabrizio Vincenzi:** Writing – original draft, Investigation, Data curation. **Anna Rita Cappello:** Validation, Supervision, Data curation. **Alessio Lodola:** Writing – original draft, Software, Formal analysis, Data curation. **Simona Saponara:** Writing – review & editing, Methodology, Formal analysis, Conceptualization. **Stefania Butini:** Writing – review & editing, Writing – original draft, Resources, Formal analysis, Conceptualization. **Gabriele Carullo:** Writing – review & editing, Writing – original draft, Investigation, Data curation, Conceptualization. **Sandra Gemma:** Writing – review & editing, Writing – original draft, Project administration, Data curation, Conceptualization. **Giuseppe Campiani:** Writing – review & editing, Writing – original draft, Supervision, Resources, Project administration, Conceptualization.

Declaration of competing interest

The authors declare that they have no known competing financial interests or personal relationships that could have appeared to influence the work reported in this paper.

Acknowledgements

Giuseppe Campiani acknowledges AIRC Project Reference AIRC 29187 CUP G43C23002760007. Giuseppe Campiani and Stefania Butini thank Next Generation EU—National Recovery and Resilience Plan (NRRP)—Mission 4 Component 2 Investment 1.4—Italian Ministry of University and Research (MUR) Project Code ECS_00000017 MUR Directoral Decree n.1055, 23 June 2022, CUP B83C22003930001, "Tuscany Health Ecosystem—THE"—Spoke 7. PRIN P2022F3YRF; EPIMET F/310034/03/X56; A.M.O.R.E., Fondazione Bartolo Longo III Millennio; IDEA - CUP: B63C22001470005; NRR-MAD-2022-12376723; DARIA - CUP: B73C22001250006; MEDUSA - CUP: B63C22002450007; UMEN - CUP: B83C22003920001; MUR-PRIN/PNRR2022:P20225KJ5L; MUR-PRIN2022A93K7S; This work was funded by the National Plan for NRRP Complementary Investments (PNC, established with the decree-law 6 May 2021, n. 59, converted by law n. 101 of 2021) in the call for the funding of research initiatives for technologies and innovative trajectories in the health and care sectors (Directorial Decree n. 931 of 06-06-2022) - project n. PNC0000003 - AdvaNced Technologies for Human-centrEd Medicine (project acronym: ANTHEM); Progetto e-DAY: Ecosistema digitale per analisi integrate di dati sanitari eterogenei relative a patologie ad alto impatto: modello innovative di assistenza e di ricerca T2-AN-21 Ministero della Salute. Anna Rita Cappello acknowledges National Recovery and Resilience Plan (NRRP) - Mission 4 Component C2 Investment 1.1 - "Fondo per il Programma Nazionale di Ricerca e Progetti di Rilevante Interesse Nazionale (PRIN)"; project code: P2022BLSMY.

Appendix A. Supplementary data

Supplementary data to this article can be found online at https://doi.org/10.1016/j.bioorg.2025.109085.

Data availability

Data will be made available on request.

References

[1] G. Carullo, S. Federico, N. Relitti, S. Gemma, S. Butini, G. Campiani, Retinitis Pigmentosa and retinal degenerations: deciphering pathways and targets for drug discovery and development, ACS Chem. Neurosci. 11 (2020) 2173–2191, https://doi.org/10.1021/acschemneuro.0c00358.

[2] A. Fontana, I. Cursaro, G. Carullo, S. Gemma, S. Butini, G. Campiani, A Therapeutic Perspective of HDAC8 in Different Diseases: An Overview of Selective Inhibitors, Int. J. Mol. Sci. 23 (2022) 10014, https://doi.org/10.3390/IJMS231710014.

[3] S. Rossi, V. Tatangelo, M. Dichiara, S. Butini, S. Gemma, S. Brogi, S. Pasquini, M. Cappello, F. Vincenzi, K. Varani, L. Lopresti, M. Malchiodi, C. Carrara, A. Gozzetti, M. Bocchia, G. Marotta, L. Patrussi, G. Carullo, C.T. Baldari, G. Campiani, A novel potent class I HDAC inhibitor reverses the STAT4/p66Shc apoptotic defect in B cells from chronic lymphocytic leukemia patients, Biomed. Pharmacother. 174 (2024) 116537, https://doi.org/10.1016/J.BIOPHA.2024.116537.

[4] N. Relitti, A.P. Saraswati, G. Chemi, M. Brindisi, S. Brogi, D. Herp, K. Schmidtkunz, F. Saccoccia, G. Ruberti, C. Ulivieri, F. Vanni, F. Sarno, L. Altucci, S. Lamponi, M. Jung, S. Gemma, S. Butini, G. Campiani, Novel quinolone-based potent and selective HDAC6 inhibitors: synthesis, molecular modeling studies and biological investigation, Eur. J. Med. Chem. 90 (2020) 112998, https://doi.org/10.1016/j.ejmech.2020.112998.

[5] G. Carullo, S. Rossi, V. Giudice, A. Pezzotta, U. Chianese, P. Scala, S. Carbone, A. Fontana, G. Panzeca, S. Pasquini, C. Contri, S. Gemma, A. Ramunno, S. Saponara, F. Galvani, A. Lodola, M. Mor, R. Benedetti, C. Selleri, K. Varani, S. Butini, L. Altucci, F. Vincenzi, A. Pistocchi, G. Campiani, Development of epigenetic modifiers with therapeutic potential in FMS-related tyrosine kinase 3/internal tandem duplication (FLT3/ITD) acute myeloid leukemia and other blood malignancies, ACS Pharmacol Transl Sci 7 (2024) 2125–2142, https://doi.org/10.1021/ACSPTSCI.4C00208.

[6] T.C.S. Ho, A.H.Y. Chan, A. Ganesan, Thirty Years of HDAC Inhibitors: 2020 Insight and hindsight, J. Med. Chem. 63 (2020) 12460–12484, https://doi.org/10.1021/acs.jmedchem.0c00830.

[7] R. Chen, M. Zhang, Y. Zhou, W. Guo, M. Yi, Z. Zhang, Y. Ding, Y. Wang, The application of histone deacetylases inhibitors in glioblastoma, J. Exp. Clin. Cancer Res. 39 (2020) 1–18, https://doi.org/10.1186/S13046-020-01643-6.

[8] M. Phimmachanh, J.Z.R. Han, Y.E.I. O'Donnell, S.L. Latham, D.R. Croucher, Histone deacetylases and histone deacetylase inhibitors in neuroblastoma, Front. Cell Dev. Biol. 8 (2020) 578770, https://doi.org/10.3389/FCELL.2020.578770.

[9] J.Y.; Kim, H.; Cho, J.; Yoo, G.W.; Kim, Y.H.; Jeon, S.W.; Lee, Y. Li, K. Deka, J.Y. Kim, H. Cho, J. Yoo, W. Kim, Y.H. Jeon, S.W. Lee, S.H. Kwon, Pathological Role of HDAC8: Cancer and Beyond, Cells 2022, Vol. 11, Page 3161 11 (2022) 3161. doi: https://doi.org/10.3390/CELLS11193161.

[10] L. Zhang, Y. Yang, Y. Li, C. Wang, C. Bian, H. Wang, F. Wang, Epigenetic regulation of histone modifications in glioblastoma: recent advances and therapeutic insights, Biomarker Research 2025 13:1 13 (2025) 1–32. doi: https://doi.org/10.1186/S40364-025-00788-W.

[11] H. Cho, E. Lee, J. Kim, S. Shin, Y.J. Kim, H. Lee, J.H. Yu, Y.H. Jeon, S.W. Lee, S. Y. Lee, K.W. Park, J.S. Kang, S.H. Kwon, Y. Kim, R. Jeon, Discovery of organosulfur-based selective HDAC8 inhibitors with anti-neuroblastoma activity, Eur. J. Pharm. Sci. 203 (2024) 106921, https://doi.org/10.1016/J.EJPS.2024.106921.

[12] I. Santos-Barriopedro, Y. Li, S. Bahl, E. Seto, Hdac8 affects mgmt levels in glioblastoma cell lines via interaction with the proteasome receptor adrm1, Genes Cancer 10 (2019) 119–133, https://doi.org/10.18632/GENESANDCANCER.197.

[13] C. Yin, P. Li, Growth suppression of glioma cells using HDAC6 inhibitor, tubacin, Open Medicine (Poland) 13 (2018) 221–226, https://doi.org/10.1515/MED-2018-0034.

[14] H. Losson, M. Schnekenburger, M. Dicato, M. Diederich, Natural Compound Histone Deacetylase Inhibitors (HDACi): Synergy with Inflammatory Signaling Pathway Modulators and Clinical Applications in Cancer, Molecules 21 (2016) 1608, https://doi.org/10.3390/MOLECULES21111608.

[15] I. Cursaro, L. Milioni, K. Eslami, H. Sirous, G. Carullo, S. Gemma, S. Butini, G. Campiani, Targeting N-methyl-lysine histone demethylase KDM4 in Cancer: natural products inhibitors as a driving force for epigenetic drug discovery, ChemMedChem 20 (2025) e202400682, https://doi.org/10.1002/CMDC.202400682.

[16] A. Wahi, P. Jain, A. Sinhari, H.R. Jadhav, Progress in discovery and development of natural inhibitors of histone deacetylases (HDACs) as anti-cancer agents, Naunyn Schmiedeberg's Arch. Pharmacol. 397 (2023) 675–702, https://doi.org/10.1007/S00210-023-02674-4.

[17] C. Seidel, M. Schnekenburger, A. Mazumder, M.H. Teiten, G. Kirsch, M. Dicato, M. Diederich, 4-Hydroxybenzoic acid derivatives as HDAC6-specific inhibitors modulating microtubular structure and HSP90α chaperone activity against prostate cancer, Biochem. Pharmacol. 99 (2016) 31–52, https://doi.org/10.1016/J.BCP.2015.11.005.

[18] T. Senawong, S. Misuna, S. Khaopha, S. Nuchadomrong, P. Sawatsitang, C. Phaosiri, A. Surapaitoon, B. Sripa, Histone deacetylase (HDAC) inhibitory and antiproliferative activities of phenolic-rich extracts derived from the rhizome of Hydnophytum formicarum Jack.: Sinapinic acid acts as HDAC inhibitor, BMC Complement. Altern. Med. 13 (2013) 1–11, https://doi.org/10.1186/1472-6882-13-232.

[19] M. Lernoux, M. Schnekenburger, M. Dicato, M. Diederich, Anti-cancer effects of naturally derived compounds targeting histone deacetylase 6-related pathways, Pharmacol. Res. 129 (2018) 337–356, https://doi.org/10.1016/J.PHRS.2017.11.004.

[20] M. Patil, A.S. Choudhari, S. Pandita, M.A. Islam, P. Raina, R. Kaul-Ghanekar, Cinnamaldehyde, cinnamic acid, and cinnamyl alcohol, the bioactives of Cinnamomum cassia exhibit HDAC8 inhibitory activity: an in vitro and in silico study, Pharmacogn. Mag. 13 (2017) S645–S651, https://doi.org/10.4103/pm.pm_389_16.

[21] M. Mahajan, S. Suryavanshi, S. Bhowmick, F.A. Alasmary, T.M. Almutairi, M. A. Islam, R. Kaul-Ghanekar, Matairesinol, an active constituent of HC9 polyherbal formulation, exhibits HDAC8 inhibitory and anticancer activity, Biophys. Chem. 273 (2021) 106588, https://doi.org/10.1016/J.BPC.2021.106588.

[22] G. Carullo, S. Mazzotta, A. Koch, K.M. Hartmann, O. Friedrich, D.F. Gilbert, M. Vega-Holm, R. Schneider-Stock, F. Aiello, New oleoyl hybrids of natural antioxidants: synthesis and in vitro evaluation as inducers of apoptosis in colorectal cancer cells, Antioxidants 9 (2020) 1–16, https://doi.org/10.3390/antiox9111077.

[23] G. Campiani, T. Khan, C. Ulivieri, L. Staiano, C. Papulino, S. Magnano, S. Nathwani, A. Ramunno, D. Lucena-Agell, N. Relitti, S. Federico, L. Pozzetti, G. Carullo, A. Casagni, S. Brogi, F. Vanni, P. Galatello, M. Ghanim, N. McCabe, S. Lamponi, M. Valoti, O. Ibrahim, J. O'Sullivan, R. Turkington, V.P. Kelly, R. VanWemmel, J.F. Díaz, S. Gemma, D. Zisterer, L. Altucci, A. De Matteis, S. Butini, R. Benedetti, Design and synthesis of multifunctional microtubule targeting agents endowed with dual pro-apoptotic and anti-autophagic efficacy, Eur. J. Med. Chem. 235 (2022) 114274, https://doi.org/10.1016/J.EJMECH.2022.114274.

[24] N. Relitti, A. Prasanth Saraswati, G. Carullo, A. Papa, A. Monti, R. Benedetti, E. Passaro, S. Brogi, V. Calderone, S. Butini, S. Gemma, L. Altucci, G. Campiani, N. Doti, Design and synthesis of Oligopeptidic Parvulin inhibitors, ChemMedChem 17 (2022) e202200050, https://doi.org/10.1002/CMDC.202200050.

[25] G. Carullo, S. Mazzotta, J. Ceramella, D. Iacopetta, A. Ramunno, C. Rosano, A. Brizzi, G. Campiani, F. Aiello, M.S. Sinicropi, Development of 1-(2-aminophenyl)pyrrole-based amides acting as human topoisomerase I inhibitors, Arch Pharm (Weinheim) 356 (2023) 2300270, https://doi.org/10.1002/ARDP.202300270.

[26] M.M. Hassan, J. Israelian, N. Nawar, G. Ganda, P. Manaswiyoungkul, Y.S. Raouf, D. Armstrong, A. Sedighi, O.O. Olaoye, F. Erdogan, A.D. Cabral, F. Angeles, R. Altintas, E.D. De Araujo, P.T. Gunning, Characterization of Conformationally constrained Benzanilide scaffolds for potent and selective HDAC8 targeting, J. Med. Chem. 63 (2020) 8634–8648, https://doi.org/10.1021/ACS.JMEDCHEM.0C01025.

[27] S. Butini, M. Brindisi, S. Brogi, S. Maramai, E. Guarino, A. Panico, A. Saxena, V. Chauhan, R. Colombo, L. Verga, E. De Lorenzi, M. Bartolini, V. Andrisano, E. Novellino, G. Campiani, S. Gemma, Multifunctional cholinesterase and amyloid Beta fibrillization modulators. Synthesis and Biological Investigation, ACS Med. Chem. Lett. 4 (2013) 1178–1182, https://doi.org/10.1021/ML4002908.

[28] S. Brogi, A. Ramunno, L. Savi, G. Chemi, G. Alfano, A. Pecorelli, E. Pambianchi, P. Galatello, G. Compagnoni, F. Focher, G. Biamonti, G. Valacchi, S. Butini, S. Gemma, G. Campiani, M. Brindisi, First dual AK/GSK-3β inhibitors endowed with antioxidant properties as multifunctional, potential neuroprotective agents, Eur. J. Med. Chem. 138 (2017) 438–457, https://doi.org/10.1016/j.ejmech.2017.06.017.

[29] F. Aiello, G. Carullo, M. Badolato, A. Brizzi, TRPV1–FAAH–COX: the couples game in pain treatment, ChemMedChem (2016) 1686–1694, https://doi.org/10.1002/cmdc.201600111.

[30] G. Carullo, A. Ahmed, A. Trezza, O. Spiga, A. Brizzi, S. Saponara, F. Fusi, F. Aiello, A multitarget semi-synthetic derivative of the flavonoid morin with improved in vitro vasorelaxant activity: role of CaV1.2 and KCa1.1 channels, Biochem. Pharmacol. 185 (2021) 114429, https://doi.org/10.1016/j.bcp.2021.114429.

[31] A.T. Negmeldin, J.R. Knoff, M.K.H. Pflum, The structural requirements of histone deacetylase inhibitors: C4-modified SAHA analogs display dual HDAC6/HDAC8 selectivity, Eur. J. Med. Chem. 143 (2018) 1790–1806, https://doi.org/10.1016/J.EJMECH.2017.10.076.

[32] S. Federico, T. Khan, A. Fontana, S. Brogi, R. Benedetti, F. Sarno, G. Carullo, A. Pezzotta, A.P. Saraswati, E. Passaro, L. Pozzetti, A. Papa, N. Relitti, S. Gemma, S. Butini, A. Pistocchi, A. Ramunno, F. Vincenzi, K. Varani, V. Tatangelo, L. Patrussi, C.T. Baldari, S. Saponara, B. Gorelli, S. Lamponi, M. Valoti, F. Saccoccia, M. Giannaccari, G. Ruberti, D. Herp, M. Jung, L. Altucci, G. Campiani, Azetidin-2-one-based small molecules as dual hHDAC6/HDAC8 inhibitors: investigation of their mechanism of action and impact of dual inhibition profile on cell viability, Eur. J. Med. Chem. 238 (2022) 114409, https://doi.org/10.1016/J.EJMECH.2022.114409.

[33] A. Papa, I. Cursaro, L. Pozzetti, C. Contri, M. Cappello, S. Pasquini, G. Carullo, A. Ramunno, S. Gemma, K. Varani, S. Butini, G. Campiani, F. Vincenzi, Pioneering first-in-class FAAH-HDAC inhibitors as potential multitarget neuroprotective agents, Arch Pharm (Weinheim) 356 (2023) 2300410, https://doi.org/10.1002/ARDP.202300410.

[34] G. Carullo, N. Orsini, I. Piano, L. Pozzetti, A. Papa, A. Fontana, D. Napoli, F. Corsi, B. Di Marco, A. Galante, L. Marotta, G. Panzeca, J. O'Brien, A.G. Sanchez, H. Doherty, N. Mahon, L. Clarke, C. Contri, S. Pasquini, B. Gorelli, S. Saponara, M. Valoti, F. Vincenzi, K. Varani, A. Ramunno, S. Brogi, S. Butini, S. Gemma, B. N. Kennedy, C. Gargini, E. Strettoi, G. Campiani, Targeting relevant HDACs to support the survival of cone photoreceptors in inherited retinal diseases:

identification of a potent pharmacological tool with in vitro and in vivo efficacy, J. Med. Chem. (2024), https://doi.org/10.1021/ACS.JMEDCHEM.4C00477.
[35] D.E. Olson, F.F. Wagner, T. Kaya, J.P. Gale, N. Aidoud, E.L. Davoine, F. Lazzaro, M. Weïwer, Y.L. Zhang, E.B. Holson, Discovery of the first histone deacetylase 6/8 dual inhibitors, J. Med. Chem. 56 (2013) 4816–4820, https://doi.org/10.1021/JM400390R.
[36] S. Gemma, G. Campiani, S. Butini, G. Kukreja, S.S. Coccone, B.P. Joshi, M. Persico, V. Nacci, I. Fiorini, E. Novellino, E. Fattorusso, O. Taglialatela-Scafati, L. Savini, D. Taramelli, N. Basilico, S. Parapini, G. Morace, V. Yardley, S. Croft, M. Coletta, S. Marini, C. Fattorusso, Clotrimazole Scaffold as an Innovative Pharmacophore Towards Potent Antimalarial Agents: Design, Synthesis, and Biological and Structure–Activity Relationship Studies, J. Med. Chem. 51 (2008) 1278–1294, https://doi.org/10.1021/JM701247K.
[37] J.D. Osko, D.W. Christianson, Structural determinants of affinity and selectivity in the binding of inhibitors to histone deacetylase 6, Bioorg. Med. Chem. Lett. 30 (2020) 127023, https://doi.org/10.1016/J.BMCL.2020.127023.
[38] Y. Hai, D.W. Christianson, Histone deacetylase 6 structure and molecular basis of catalysis and inhibition, Nat. Chem. Biol. 12 (2016) 741–747, https://doi.org/10.1038/nchembio.2134.
[39] N.J. Porter, A. Mahendran, R. Breslow, D.W. Christianson, Unusual zinc-binding mode of HDAC6-selective hydroxamate inhibitors, Proc. Natl. Acad. Sci. USA 114 (2017) 13459–13464, https://doi.org/10.1073/PNAS.1718823114.
[40] M.T. Tavares, L.C. de Almeida, T. Kronenberger, G. Monteiro Ferreira, T. Fujii de Divitiis, M. Franco Zannini Junqueira Toledo, N. Mariko Aymoto Hassimotto, J. Agostinho Machado-Neto, L. Veras Costa-Lotufo, R. Parise-Filho, Structure-activity relationship and mechanistic studies for a series of cinnamyl hydroxamate histone deacetylase inhibitors, Bioorg. Med. Chem. 35 (2021) 116085, https://doi.org/10.1016/J.BMC.2021.116085.
[41] J. Choi, J. Hwang, M. Ramalingam, H.S. Jeong, S. Jang, Effects of HDAC inhibitors on neuroblastoma SH-SY5Y cell differentiation into mature neurons via the Wnt signaling pathway, BMC Neurosci. 24 (2023) 1–10, https://doi.org/10.1186/S12868-023-00798-0.
[42] H. Jin, L. Liang, L. Liu, W. Deng, J. Liu, HDAC inhibitor DWP0016 activates p53 transcription and acetylation to inhibit cell growth in U251 glioblastoma cells, J. Cell. Biochem. 114 (2013) 1498–1509, https://doi.org/10.1002/JCB.24491.
[43] J.R. Mekala, R.K. Kurappalli, P.S. Ramalingam, N.R. Moparthi, N-acetyl l-aspartate and Triacetin modulate tumor suppressor MicroRNA and class I and II HDAC gene expression induce apoptosis in glioblastoma cancer cells in vitro, Life Sci. 286 (2021) 120024, https://doi.org/10.1016/J.LFS.2021.120024.
[44] E. White, R.S. DiPaola, The double-edged sword of autophagy modulation in cancer, Clin. Cancer Res. 15 (2009) 5308–5316, https://doi.org/10.1158/1078-0432.
[45] N. Gammoh, D. Lam, C. Puente, I. Ganley, P.A. Marks, X. Jiang, Role of autophagy in histone deacetylase inhibitor-induced apoptotic and nonapoptotic cell death, Proc. Natl. Acad. Sci. USA 109 (2012) 6561–6565, https://doi.org/10.1073/PNAS.1204429109.
[46] A. Pouyan, M. Ghorbanlo, M. Eslami, M. Jahanshahi, E. Ziaei, A. Salami, K. Mokhtari, K. Shahpasand, N. Farahani, T.E. Meybodi, M. Entezari, A. Taheriazam, K. Hushmandi, M. Hashemi, Glioblastoma multiforme: insights into pathogenesis, key signaling pathways, and therapeutic strategies, Mol. Cancer 24 (2025) 1–51, https://doi.org/10.1186/S12943-025-02267-0.
[47] J. Auzmendi-Iriarte, A. Saenz-Antoñanzas, I. Mikelez-Alonso, E. Carrasco-Garcia, M. Tellaetxe-Abete, C.H. Lawrie, N. Sampron, A.L. Cortajarena, A. Matheu, Characterization of a new small-molecule inhibitor of HDAC6 in glioblastoma, Cell Death Dis. 11 (6) (2020) 1–14, https://doi.org/10.1038/s41419-020-2586-x.
[48] X. Qian, G. Ara, E. Mills, W.J. LaRochelle, H.S. Lichenstein, M. Jeffers, Activity of the histone deacetylase inhibitor belinostat (PXD101) in preclinical models of prostate cancer, Int. J. Cancer 122 (2008) 1400–1410, https://doi.org/10.1002/IJC.23243.
[49] J. Xu, D. Sampath, F.F. Lang, S. Prabhu, G. Rao, G.N. Fuller, Y. Liu, V.K. Puduvalli, Vorinostat modulates cell cycle regulatory proteins in glioma cells and human glioma slice cultures, J. Neuro-Oncol. 105 (2011) 241–251, https://doi.org/10.1007/S11060-011-0604-7.
[50] B. Gabrielli, M. Brown, Histone deacetylase inhibitors disrupt the mitotic spindle assembly checkpoint by targeting histone and nonhistone proteins, Adv. Cancer Res. 116 (2012) 1–37, https://doi.org/10.1016/B978-0-12-394387-3.00001-X.
[51] F.E. Stevens, H. Beamish, R. Warrener, B. Gabrielli, Histone deacetylase inhibitors induce mitotic slippage, Oncogene 27 (2008) 1345–1354, https://doi.org/10.1038/SJ.ONC.1210779.
[52] Y. Myung, A.G.C. De Sá, D.B. Ascher, Deep-PK: deep learning for small molecule pharmacokinetic and toxicity prediction, Nucleic Acids Res. 52 (2024) W469–W475, https://doi.org/10.1093/NAR/GKAE254.
[53] D. Palmieri, P.R. Lockman, F.C. Thomas, E. Hua, J. Herring, E. Hargrave, M. Johnson, N. Flores, Y. Qian, E. Vega-Valle, K.S. Taskar, V. Rudraraju, R. K. Mittapalli, J.A. Gaasch, K.A. Bohn, H.R. Thorsheim, D.J. Liewehr, S. Davis, J. F. Reilly, R. Walker, J.L. Bronder, L. Feigenbaum, S.M. Steinberg, K. Camphausen, P.S. Meltzer, V.M. Richon, Q.R. Smith, P.S. Steeg, Vorinostat inhibits brain metastatic colonization in a model of triple-negative breast cancer and induces DNA double-strand breaks, Clin. Cancer Res. 15 (2009) 6148–6157, https://doi.org/10.1158/1078-0432.CCR-09-1039/347357.
[54] E.Q. Lee, V.K. Puduvalli, J.M. Reid, J.G. Kuhn, K.R. Lamborn, T.F. Cloughesy, S. M. Chang, J. Drappatz, W.K.A. Yung, M.R. Gilbert, H.I. Robins, F.S. Lieberman, A. B. Lassman, R.M. McGovern, J. Xu, S. Desideri, X. Ye, M.M. Ames, I. Espinoza-Delgado, M.D. Prados, P.Y. Wen, Phase I study of vorinostat in combination with temozolomide in patients with high-grade gliomas: north american brain tumor consortium study 04-03, Clin. Cancer Res. 18 (2012) 6032–6039, https://doi.org/10.1158/1078-0432.CCR-12-1841/286479.
[55] A.S. Guntner, A. Peyrl, L. Mayr, B. Englinger, W. Berger, I. Slavc, W. Buchberger, J. Gojo, J. Gojo, Cerebrospinal fluid penetration of targeted therapeutics in pediatric brain tumor patients, Acta Neuropathol. Commun. 8 (2020) 1–13, https://doi.org/10.1186/S40478-020-00953-2.
[56] D.H. Lee, H.-W. Ryu, H.-R. Won, S.H. Kwon, D.H. Lee, H.-W. Ryu, H.-R. Won, S. H. Kwon, Advances in epigenetic glioblastoma therapy, Oncotarget 8 (2017) 18577–18589, https://doi.org/10.18632/ONCOTARGET.14612.
[57] L. Zaccagnini, S. Brogi, M. Brindisi, S. Gemma, G. Chemi, G. Legname, G. Campiani, S. Butini, Identification of novel fluorescent probes preventing PrPSc replication in prion diseases, Eur. J. Med. Chem. 127 (2017) 859–873, https://doi.org/10.1016/J.EJMECH.2016.10.064.
[58] Life Science: MacroModel - Schrödinger, (n.d.). https://newsite.schrodinger.com/platform/products/macromodel/ (accessed March 2, 2024).
[59] C. Lu, C. Wu, D. Ghoreishi, W. Chen, L. Wang, W. Damm, G.A. Ross, M.K. Dahlgren, E. Russell, C.D. Von Bargen, R. Abel, R.A. Friesner, E.D. Harder, OPLS4: improving force field accuracy on challenging regimes of chemical space, J. Chem. Theory Comput. 17 (2021) 4291–4300, https://doi.org/10.1021/acs.jctc.1c00302.
[60] Maestro | Schrödinger. https://www.schrodinger.com/platform/products/maestro/, 2025 accessed June 4, 2025.
[61] Glide — glide v0.9.1, (2025). https://hexdocs.pm/glide/Glide.html (accessed June 4, 2025).
[62] E. Chiaino, R. Stella, C. Peggion, M. Micucci, R. Budriesi, L.B. Mattioli, C. Marzetti, F. Pessina, M. Valoti, M. Frosini, Acacia catechu willd. Extract protects neuronal cells from oxidative stress-induced damage, Antioxidants 11 (2022) 81, https://doi.org/10.3390/ANTIOX11010081/S1.
[63] A. Fontana, L. Bergantini, G. Carullo, L. Scalvini, M. D'Alessandro, C. Papulino, P. Cameli, S. Gangi, F. Vincenzi, K. Varani, C. Contri, S. Pasquini, A. Pistocchi, A. Pezzotta, S. Carbone, S. Saponara, S. Gemma, L. Altucci, R. Benedetti, A. Lodola, M. Mor, E. Bargagli, S. Butini, G. Campiani, Spirotetrahydroisoquinoline-based histone deacetylase inhibitors as new Antifibrotic agents: biological evaluation in human fibroblasts from Bronchoalveolar lavages of idiopathic pulmonary fibrosis patients, ACS Pharmacol Transl Sci (2024), https://doi.org/10.1021/ACSPTSCI.4C00456.
[64] G. Allavena, B. Del Bello, P. Tini, N. Volpi, G. Valacchi, C. Miracco, L. Pirtoli, E. Maellaro, Trehalose inhibits cell proliferation and amplifies long-term temozolomide- and radiation-induced cytotoxicity in melanoma cells: a role for autophagy and premature senescence, J. Cell. Physiol. 234 (2019) 11708–11721, https://doi.org/10.1002/JCP.27838.